DEUTSCHES ELEKTRONEN-SYNCHROTRON DESY

DESY 75/40
October 1975



# Review of Electroproduction of Final States

by

Günter Wolf

2 HAMBURG 52 · NOTKESTIEG 1

To be sure that your preprints are promptly included in the
HIGH ENERGY PHYSICS INDEX ,
send them to the following address ( if possible by air mail ) :

# Review of Electroproduction of Final States*

by

Günter Wolf

Deutsches Elektronen Synchrotron DESY, Hamburg, Germany

---

* Invited talk given at the 1975 International Symposium on Lepton and Photon Interactions at High Energies, Aug. 21-27, 1975, Stanford University.

## I. INTRODUCTION

A study of the final states in electroproduction can answer many questions such as

- transition form factors of the higher nucleon resonances;
- $\pi$ and K form factors;
- the $Q^2$ dependence of the direct photon-vector meson couplings;
- does the photon shrink?
- is there evidence for a constituent picture of the nucleon?

and above all:

- how do the final states in the deep inelastic region conspire to achieve scaling?

New and interesting results have been obtained on some of these questions; for others there is still no clue yet.

This review will cover exclusive final states as well as inclusive hadron spectra produced in electron or muon-nucleon scattering. In general only new experimental data will be discussed. Some of these have already been reviewed in Ref. 1, or described at this conference[2]. Summaries of previous measurements can be found e.g. in Ref. 3.

## 2. NOTATION

The analysis of the experimental data assumes one-photon exchange approximation as depicted in the following diagram:

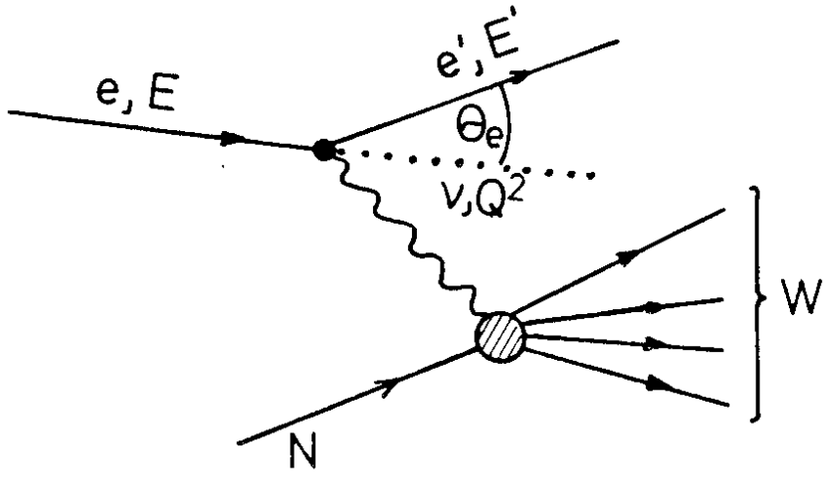

with

$\nu = E - E'$ energy of the virtual photon in the lab. system;

$Q^2 = 4EE'\sin^2\Theta_e/2$ negative mass squared of the virtual photon;

$W^2 = 2m_p\nu + m_p^2 - Q^2$ square of the total hadron c.m. energy

In terms of these quantities the scaling variables $\omega$ and $\omega'$ are defined as

$\omega = 2m_p\nu/Q^2$

$\omega' = (2m_p\nu + m_p^2)/Q^2 = W^2/Q^2 + 1$

All results will be presented in terms of the virtual $\gamma$-nucleon scattering process. The cross sections $\sigma_L, \sigma_T$ for longitudinal and transverse photon nucleon scattering are determined from the measured lepton nucleon cross section using the following relation:

$$\frac{d\sigma}{dQ^2dW} = \frac{\pi}{2EE'}\frac{W}{m_p}\,\Gamma_t\{\sigma_T(Q^2,W) + \varepsilon\,\sigma_L(Q^2,W)\}$$

where

$\Gamma_t = \frac{\alpha}{4\pi^2}\,\frac{W^2 - m_p^2}{m_p\,Q^2}\,\frac{E}{E'(1-\varepsilon)}$ measures the flux of transverse photons,

$\varepsilon = \left[1 + 2(1 + \nu^2/Q^2)\,tg^2\,\frac{\Theta_e}{2}\right]^{-1}$ is the polarization parameter ($0 \le \varepsilon \le 1$), and

$\Gamma_L = \varepsilon\Gamma_t$ is the flux of longitudinal photons.

In general no attempt is made to separate $\sigma_T$ and $\sigma_L$. The measurable sum $\sigma_T + \varepsilon\sigma_L$ is defined to be the virtual photon nucleon cross section. Because $\sigma(ep \to e'X)$ falls off rapidly with $\Theta_e$, most data have a polarization parameter $\varepsilon$ of order 0.7 - 0.9.

## 3. SINGLE PION PRODUCTION IN THE RESONANCE REGION

At DESY and NINA programs have been started to study systematically single pion production in the region of the second and third resonances. Small steps are taken in W and for each W point the $Q^2$ dependence of the pion angular distribution is measured. As an example Fig. 1 shows the W

dependence of the forward $\pi^+$ cross section at $Q^2 = 0.4$ GeV$^2$ from NINA[4] and at $Q^2 = 0.6$ and 1 GeV$^2$ from DESY[5]. A different $Q^2$ behaviour is observed for the second and third resonance regions. A series of angular distributions measured by the DESY group[5] in this kinematical region is shown in Fig. 2. For a review of the experimental situation in the resonance region see Ref. 6. Eventually these measurements should allow the unravelling of the contributions from various resonances through a phase shift analysis and the extraction of the form factors for these states[7].

## 4. CHARGED PION PRODUCTION AND THE PION FORM FACTOR

Fig. 3 summarizes the differential cross section data, $d\sigma/dt$, for

$$\gamma_V p \to \pi^+ n$$

as measured above the resonance region at DESY[8] ($Q^2 = 0.06$, 0.3 and 0.7 GeV$^2$) and by the Harvard group[9] at Cornell ($Q^2 = 1.8$ and 3.7 GeV$^2$). For $|t| \gtrsim 0.1$ GeV$^2$ a noticeable drop is observed in $d\sigma/dt$ between photoproduction and $Q^2 = 0.7$ GeV$^2$; for higher $Q^2$ values the cross section changes little with $Q^2$.

Before analysing the production mechanism we draw attention to the following rather trivial points. The first involves the increase of the minimal t value, $t_{min}$, with $Q^2$

($|t|_{min} < 0.05$ GeV$^2$ for $Q^2 < 0.7$ GeV$^2$, $|t|_{min} = 0.14$ GeV$^2$ at $Q^2 = 1.8$ GeV$^2$ and 0.4 GeV$^2$ at $Q^2 = 3.7$ GeV$^2$). Had we compared $d\sigma/d\Omega$ for a fixed scattering angle, e.g. $\Theta = 0^\circ$, rather than $d\sigma/dt$ for fixed t, a strong $Q^2$ dependence would also have been seen for $Q^2 > 0.7$ GeV$^2$. For peripheral processes therefore a representation in terms of $d\sigma/dt$ seems to be preferred over $d\sigma/d\Omega$.

Secondly, since, as in most two-body reactions, $d\sigma/dt$ is a concave function (smaller slope for larger $|t|$ values), and since $t_{min}$ increases with $Q^2$, the average transverse momentum for $\pi^+$ from $\gamma_V p \to \pi^+ n$ will grow with increasing $Q^2$.

The major contribution to peripheral $\pi^+$ production comes from one-pion exchange (see diagram).

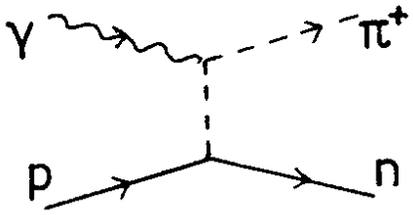


As compared to photoproduction the importance of one-pion exchange is enhanced due to the additional contribution from longitudinal photons. This is reflected by the ratio of $\pi^+$ and $\pi^-$ production on deuterons[8] (basically $\gamma n \to \pi^- p$ vs $\gamma p \to \pi^+ n$) shown in Fig. 4. For pure $\pi$ exchange this ratio has to be unity. Deviations from unity indicate isoscalar contributions. We see that at $Q^2 = 0.7$ GeV$^2$ the t range over which the $\pi^-/\pi^+$ ratio is close to one is considerably larger than for photoproduction.

The Harvard group[9] has extracted the pion form factor $F_\pi(Q^2)$ from their data using a dispersion theory model[10] to evaluate the contributions from other Born diagrams and background terms. The resulting pion charge radius agrees with those from other experiments, which use different methods:

$$\begin{aligned} \langle r_\pi \rangle^{1/2} &= 0.704 \pm 0.007 \text{ f} \quad (\gamma_V p \to \pi^+ n)^{9} \\ &= 0.78 \pm 0.09 \text{ f} \quad (\pi e \to \pi e)^{11a} \\ &= 0.73 \pm 0.13 \text{ f} \quad (\pi^- p \to e^+ \pi^- n)^{11b} \end{aligned}$$

The $Q^2$ behaviour of $F_\pi$ multiplied by a factor $Q^2$ is shown in Fig. 5. After the turn-on at low $Q^2$ the quantity $Q^2 F_\pi(Q^2)$ reaches a plateau. Such a behaviour is consistent with a one-pole description,

$$F_\pi(Q^2) = (1 + Q^2/m^2)^{-1}$$

The mass squared of the effective pole turns out to be $m^2 = 0.47 \pm 0.01$ GeV$^2$ which is somewhat lower than the square of the rho meson mass.*

---

* Speculation: If the difference is attributed to the presence of a second

The weak $Q^2$ dependence of $d\sigma/dt$ outside the peripheral peak was predicted by the authors of Ref.14 who started from a dual current model with infinitely many vector mesons. Summing over the vector mesons gives a contribution nearly independent of $Q^2$ provided $Q^2$ is small compared to s, and $|t| \gtrsim 0.5$ GeV$^2$.

## 5. $\pi^o$ ELECTROPRODUCTION

Single $\pi^o$ electroproduction, $ep \to e\pi^o p$, was studied in an experiment at DESY[15]. The rather difficult separation of this reaction from background was accomplished by detecting all final state particles. Electron and proton were measured in two magnetic spectrometers, the two photons from $\pi^o$ decay were observed in a lead glass hodoscope.

The differential cross section for the process

$$\gamma_V p \to \pi^o p$$

depends on the orientation of the $\pi^o$ production plane relative to the electron scattering plane (= plane of polarization of the transverse photons) measured by the azimuthal angle $\Phi$. The cross section can be decomposed into $d\sigma_{\parallel}/dt$ and $d\sigma_{\perp}/dt$ for $\pi^o$ emission at $\Phi = 0^o$ and $90^o$ respectively, and $d\sigma_L/dt$ and $d\sigma_I/dt$ for the longitudinal and longitudinal/transverse interference contributions :

---

pole, a $\rho(1250)$ say, one can write

$$F_\pi = \frac{1 + C}{1 + Q^2/m_\rho^2} - \frac{C}{1 + Q^2/m_{\rho'}^2},$$

and finds

$$\frac{C}{1 + C} = \frac{-g_{\gamma\rho'} f_{\rho'\pi\pi}}{g_{\gamma\rho} f_{\rho\pi\pi}} = 0.11$$

Association of the $\omega\pi^o$ bump seen in photoproduction with the $\rho(1250)$ leads to $(g_{\gamma\rho'}/g_{\gamma\rho})^2 \approx \sigma(\gamma p \to \rho^{o'} p)/\sigma(\gamma p \to \rho^o p) \approx 0.2$ [12] and finally to $\Gamma_{\rho'\pi\pi}/\Gamma_{\rho'} \approx 0.07$, a value which is not in contradiction with a recent phase shift analysis[13].

$$\frac{d^2\sigma}{dtd\Phi}(\gamma_V p \to \pi^o p) = \frac{1}{4\pi}\left\{\frac{d\sigma_{\parallel}}{dt} + \frac{d\sigma_{\perp}}{dt} + \varepsilon\cos 2\Phi\left(\frac{d\sigma_{\parallel}}{dt} - \frac{d\sigma_{\perp}}{dt}\right)\right.$$
$$\left. + 2\varepsilon\frac{d\sigma_L}{dt} + 2\cos\Phi\sqrt{2\varepsilon(\varepsilon+1)}\ \frac{d\sigma_I}{dt}\right\}$$

The experiment was carried out at $\Phi = 90^o$ where the interference contribution vanishes:

$$\frac{d^2\sigma}{dtd\Phi}(\Phi = 90^o) = \frac{1}{4\pi}\left\{(1+\varepsilon)\frac{d\sigma_{\perp}}{dt} + (1-\varepsilon)\frac{d\sigma_{\parallel}}{dt} + 2\varepsilon\frac{d\sigma_L}{dt}\right\}$$

According to the Stichel theorem, generalized to electroproduction, only natural parity exchange in the t channel contributes to $\sigma_{\perp}$ at high energies. Similarily, $\sigma_{\parallel}$ and $\sigma_L$ come only from unnatural parity exchange[16]. Since $\pi$ exchange is excluded the unnatural parity parts of the cross section are expected to be small. Therefore

$$\frac{d\sigma_{\perp}}{dt} \simeq \frac{4\pi}{1+\varepsilon}\frac{d^2\sigma}{dtd\Phi}(\Phi = 90^o)$$

(Note that $\frac{4\pi}{1+\varepsilon}\frac{d^2\sigma}{dtd\Phi}(\Phi = 90^o) \geq \frac{d\sigma_{\perp}}{dt}$ independent of these arguments). Fig. 6 shows the quantity $\frac{4\pi}{1+\varepsilon}\, d^2\sigma/dtd\Phi$ measured for W = 2.55 GeV as a function of t at $Q^2$ values of 0.22, 0.55 and 0.85 $GeV^2$. In photoproduction, $d\sigma_{\parallel}/dt$ (the solid line in Fig. 6) shows a dip at $|t| = 0.5$ $GeV^2$ followed by a second maximum around 1 $GeV^2$. The dip has been interpreted either as a nonsense zero of the vector and tensor trajectory ($\alpha(t) \simeq 0.5+t$) or as a zero of the Bessel function $J_1(R\sqrt{-t})$ where R measures the radius of interaction. It was suggested[17] that by measuring the $Q^2$ dependence of the dip position a choice could be made between the two alternatives: while the Regge zero should not move, the Bessel zero might if R changes (shrinking photon). It seems that nature does not know about this nice possibility. The second maximum and with it the dip disappear with dramatic speed: between $Q^2 = 0$ and 0.22 $GeV^2$ the cross section around $|t| = 1$ $GeV^2$ drops by a factor of ten.

In Fig. 7 the data have been replotted as a function of $Q^2$ for fixed t. The $Q^2$ dependence appears to be a rather complicated function of t. Theoretically, the observed $Q^2$ behaviour is not understood[18].

6. $\gamma_V p \to K^+\Lambda,\ K^+\Sigma^o$

A summary of cross section measurements[19,20] on

$$\gamma_V p \to K^+\Lambda$$
$$\gamma_V p \to K^+\Sigma^o$$

is given in Fig. 8 for a fixed value of W (W = 2.2 GeV) and a small range of t values ($0.1 < |t| < 0.18$ GeV$^2$). In addition there exist cross section data for other values of W,t,$Q^2$ from a Harvard-Cornell and a Harvard experiment at Cornell[21] where $K^+$ production along the virtual photon direction has been studied up to $Q^2 = 4$ GeV$^2$. There is a qualitative difference in the $Q^2$ behaviour of $K^+\Lambda$ and $K^+\Sigma^o$: the $K^+\Sigma^o$ cross section decreases rapidly with $Q^2$ while in the $K^+\Lambda$ case the $Q^2$ dependence is weak, suggesting an appreciable contribution from longitudinal photons. This is in agreement with what one naively expects: Since the $KN\Sigma$ coupling constant, $G^2_{KN\Sigma}$, is supposedly smaller than $G^2_{KN\Lambda}$ (Ref. 22) K exchange will play a minor role in $K^+\Sigma^o$ production but will contribute significantly to the $K^+\Lambda$ cross section, in particular to its longitudinal part. Bartl and Majerotto[23] have concluded that a quantitative description of both photo and electroproduction data for $K^+\Lambda$ and $K^+\Sigma^o$ requires K, $K^*$, $K^{**}$ and either $K_A(1^{+-})$ or $K_B(1^{++})$ exchange.

7. $\gamma_V p \to \pi^-\Delta^{++}$ AND THE AXIAL VECTOR FORM FACTOR

A DESY-Glasgow collaboration has studied the reaction

$$\gamma_V p \to \pi^-\Delta^{++}$$

as a function of $Q^2$ and W and in particular its behaviour near threshold[24]. The total cross section (Fig. 9) at an average $Q^2$ value of 0.6 GeV$^2$ goes through a maximum around W = 1.5 GeV and decreases rapidly at higher energies. The steep, approximately linear rise of the cross section above threshold and the flatness of the $\pi^-$ cms production angular distribution in the threshold region lead to the conclusion that s-wave production dominates. Furthermore, a study of the $\Delta^{++}$ decay angular distribution shows that the $\Delta^{++}$ has predominantly helicity $\lambda_\Delta = 3/2$. The $\pi^-\Delta^{++}$ system is therefore in a $D^-_{3/2}$ state (notation refers to a $\pi$N state). This excludes the possibility that P11 formation is responsible for $\pi^-\Delta^{++}$ pro-

duction near threshold. The observed production features are consistent with the dominance of the contact term (see diagram) expected in the model of Stichel and Scholz[25]. A similar conclusion was reached for the photoproduction data[26].

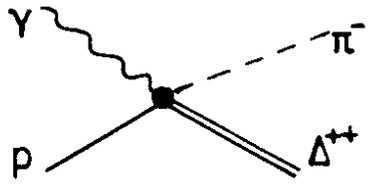


The data allow therefore a study of the $Q^2$ dependence of the contact term. Fig. 10a shows $\sigma_{\pi^-\Delta^{++}}$ versus $Q^2$ in the threshold region. Contrary to naive expectation a rapid decrease with $Q^2$ is observed. The decrease is well reproduced by multiplying the Born cross section with a factor $(1 + Q^2/m_\rho^2)^{-2}$, where $m \simeq 0.7$ GeV.[24]

In a dispersion theoretical calculation by Berends and Gastmans[27] and more recently by Levi and Schmidt[28] the contact term acquires a form factor which can be related to the N and Δ form factors. It is not yet clear whether this leads to a quantitative description of the data. Bartl, Majerotto and Schildknecht[29], in the spirit of the vector dominance model (VDM) assumed a $\rho N\pi\Delta$ contact interaction (see diagram). As a consequence the Born cross section is multiplied by a factor $(1 + Q^2/m_\rho^2)^{-2}$ which gives a quantitative description of the threshold region[24].

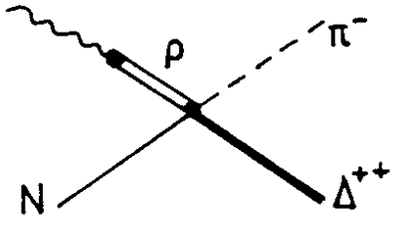


However, the model may have difficulties with the crossing symmetric reaction, $\pi^+ p \to \rho^0 \Delta^{++}$, for which the cross section predicted from the $\rho N\pi\Delta$ contact term exceeds the measured one by more than an order of magnitude unless the s-wave is almost completely absorbed.

The DESY-Glasgow collaboration has used their data to determine the axial vector N-Δ transition form factor $F_A(Q^2)$. This is possible because

at threshold where the pion cms momentum is zero the $\gamma\pi$ system is in a $1^+$ state. Extrapolation to the PCAC limit, $m_\pi \to 0$, gives the $\gamma\pi$ system a mass squared equal to $Q^2$. Fig. 10b shows $F_A(Q^2) \equiv g_A(Q^2)/g_A(0)$ and measurements of the axial vector nucleon form factor determined in a similar manner from $ep \to e\pi^+n$ near threshold[31-33]. Both sets of data can be parametrized by a dipole,

$$F_A(Q^2) = (1 + Q^2/m_A^2)^{-2}$$

with $m_A = (1.17 \pm 0.03)$ GeV.[24] There is a discrepancy, however, with the direct determination of $F_A$ from $\nu p$ scattering which leads to $m_A = 0.89 \pm 0.08$ GeV.[34] The origin of this discrepancy is not yet known.

In conclusion, the $Q^2$ dependence of the contact term contribution is likely to be determined by both the axial vector form factor $F_A$ and the vector form factors $F_V$ of N and $\Delta$. Even in the PCAC limit ($q_\pi \to 0$, $m_\pi^2 \to 0$) the influence of $F_V$ may be nonnegligible since one is far from the nearest axial vector pole. Therefore, in order to interpret the observed $Q^2$ dependence of the contact interaction a unified theoretical treatment in terms of $F_A$ and $F_V$ is required.

## 8. VECTOR MESON PRODUCTION

### a) $\gamma_V p \to \rho^o p$

In Fig. 11 the $\pi^+\pi^-$ mass spectrum is shown for the reaction $\gamma_V p \to \pi^+\pi^- p$ as measured by the DESY-Glasgow collaboration[35]. A strong rho signal is observed. Little background is left when small momentum transfer events are selected (shaded histogram).

### $Q^2$ DEPENDENCE OF THE $\rho^o$ CROSS SECTION

Fig. 12 summarizes the $\rho^o$ cross section measured in the threshold region and for W > 2 GeV as a function of $Q^2$. The data come from four different experiments. In the experiments of the DESY-Glasgow[35] and the Santa Cruz-SLAC[36] collaborations streamer chambers were employed. The SLAC spark chamber experiment detected the scattered electron and $\pi^+$ and $\pi^-$ in spark chambers[37]. The Cornell experiment measured e' and p in two spectrometers and determined the sum of $\rho$ and $\omega$ production from an analysis of the

missing-mass spectrum[38]. From this the rho cross section, $\sigma_\rho$, was obtained by assuming the ratio $\sigma_\omega/\sigma_\rho$ to be the same as in photoproduction.

In Fig. 12 $\sigma_\rho(Q^2)/\sigma_\rho(0)$ rather than $\sigma_\rho(Q^2)$ has been plotted. In this way most of the W dependence is taken out and the comparison between experiments averaged over different values of W is facilitated. For $W > 2$ GeV where most of the data have been taken the agreement among the experiments is good. These data show a rapid decrease of $\sigma_\rho$ with increasing $Q^2$. At $Q^2 \approx 1$ GeV$^2$ $\sigma_\rho(Q^2)$ is down by a factor of ~10 from its photoproduction value. Only 20-30 % of this drop is caused by the $t_{min}$ cut off. A somewhat different $Q^2$ behaviour is observed in the threshold region ($1.7 < W < 2$ GeV). For $Q^2$ values between 0.3 and 0.8 GeV$^2$ the decrease with $Q^2$ is much less pronounced.

The solid curves in Fig. 12 show the VDM prediction (see diagram)

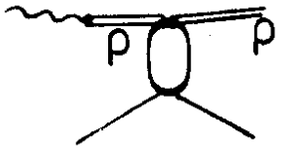


including corrections for the difference in photon flux, for the $t_{min}$ cut off and for longitudinal photon contributions[35];

$$\sigma_\rho^{VDM}(Q^2) = \frac{p^*_{in}(Q^2=0)}{p^*_{in}(Q^2)} \frac{(1 + \varepsilon\xi^2 Q^2/m_\rho^2)}{(1 + Q^2/m_\rho^2)^2} \exp\left[A(t_{min}(Q^2) - t_{min}(0))\right] \sigma_\rho(0)$$

where

$$p^*_{in}(0)/p^*_{in}(Q^2) = (W^2 - m_p^2)/\{(W^2 - m_p^2 - Q^2)^2 + 4W^2Q^2\}^{1/2} \quad .$$

The quantity $\xi^2Q^2/m_\rho^2$ measures the ratio of $\rho$ production by longitudinal and transverse photons (see below).

Near threshold and for $Q^2 < 1$ GeV$^2$ the $\sigma_\rho$ predicted by VDM is smaller than the measured values. For higher energies where $\rho$ production becomes mainly diffractive the VDM prediction agrees with the data. This result is of some importance: it means for example that the failure of the simple VDM (only $\rho$,$\omega$, and $\Phi$) to account for the total $\gamma_V p$ cross section in the deep inelastic region is probably not caused by an additional

$Q^2$ dependence of either the $\gamma V$ coupling or the VN forward scattering amplitude.

A triple Regge description of rho electroproduction assuming VDM can be found in Ref. 39.

In the massive quark model of Preparata[40] the $Q^2$ dependence of the cross section obeys a scaling law:

$$\frac{d\sigma}{dt}(\gamma_V p \to \rho^o p) = \frac{1}{(Q^2 + m_\rho^2)^3} F(x_\rho)\, e^{2\lambda(x_\rho)t}$$

where $x_\rho = (Q^2 + m_\rho^2)/2\nu$ and $F(x_\rho)$, $\lambda(x_\rho)$ are unknown functions. This leads to*

$$(Q^2 + m_\rho^2)^3\, \sigma(\gamma_V p \to \rho^o p) = G(x_\rho)$$

where G is a function of $x_\rho$ alone. The data, in particular the rise of the cross section in the threshold region, are consistent with this scaling law. It will be interesting to test this proposal over a large $Q^2$ and W range.

t DEPENDENCE OF $\gamma_V p \to \rho^o p$

The differential cross section for moderately small values of t is of the form

$$d\sigma/dt \sim \exp(A_{\rho p} t)$$

In an optical model the slope A measures the radius of interaction, $A = R^2_{\gamma p}/4$ with $R^2_{\gamma p} = R^2_\gamma + R^2_p$. If the photon shrinks[41] with increasing $Q^2$ one should observe a decrease of $A_{\rho p}$. Shrinkage may occur e.g. if the time $\Delta\tau$ allowed by the uncertainty relation for the photon to turn into a rho is less than it takes the photon to traverse a nucleon:

$$\frac{2\nu}{Q^2 + m_\rho^2} < 10\ \text{GeV}^{-1}$$

For a definite test on shrinkage the transverse and longitudinal photon contributions have to be analyzed separately. This has not yet been done.

---

* neglecting $t_{min}$ effects

Fig. 13 shows photo-[42] and electroproduction measurements[35-37,43] of $A_{\rho p}$ as a function of $\Delta\tau$ for $d\sigma_T/dt + \varepsilon\, d\sigma_L/dt$. The data of Ref. 38 were not included because of the contamination by $\omega$ production. No significant difference between photo and electroproduction data, i.e. no shrinkage effect is observed. However in the "threshold" region ($\Delta\tau < 10\ GeV^{-1}$) the accuracy of the data is insufficient to exclude even maximal shrinkage, $R_\gamma \to 0$ or $A_{\rho p} \to \frac{1}{2} A_{pp} \simeq 5\ GeV^{-2}$ as $\Delta\tau \to 0$.

SPIN DEPENDENCE OF $\gamma_V p \to \rho^o p$

In the experiments of Refs. 35-37 and 43 the $\rho^o$ decay angular distribution was measured and analysed in terms of the $\rho^o$ spin density matrix[44]. The shape of the polar angle distribution is determined by the value of the density matrix element $r_{oo}^{o4}$ ($0 < r_{oo}^{o4} < 1$; in the limit $Q^2 \to 0$: $r_{oo}^{o4} \to \rho_{oo}$):

$$W(\cos\Theta) \sim (1 - r_{oo}^{o4}) + (3r_{oo}^{o4} - 1)\cos^2\Theta$$

Purely longitudinal rhos are characterized by $r_{oo}^{o4} = 1$, transverse rhos have $r_{oo}^{o4} = 0$. Fig. 14a shows the energy dependence of $r_{oo}^{o4}$ at $Q^2 = 0$ (ABBHHM[45]) and $\langle Q^2 \rangle = 0.7\ GeV^2$ (DESY-Glasgow[35], SLAC[43]). In both, photo and electroproduction more longitudinal than transverse rhos are being produced close to threshold. With increasing W the fraction of longitudinal rhos drops rapidly. In photoproduction $r_{oo}^{o4}$ is close to zero for $W > 2$ GeV; in electroproduction $r_{oo}^{o4}$ approaches a constant value of 0.2 to 0.3.

From a study of the full density matrix the DESY-Glasgow collaboration[35] concludes that for $W > 2.2$ GeV and $|t| < 0.5\ GeV^2$ rho production conserves the s-channel helicity to good accuracy. The amplitude for a single flip in phase with the non-flip amplitude is less than 10 % of the non-flip amplitude. The longitudinal and transverse photon amplitudes are found to interfere. Fig. 14b shows the phase $\delta$ between the two helicity amplitudes ($T_{\lambda_\rho \lambda_\gamma}$):

$$T_{oo} T_{11}^* = |T_{oo}||T_{11}|\, e^{-i\delta}$$

With increasing energy the longitudinal and transverse amplitudes become more and more in phase.

Assuming SCHC, longitudinal rhos are produced by longitudinal photons only and transverse rhos only by transverse photons. The ratio R between the cross sections can be calculated directly from $r_{oo}^{o4}$:

$$R \equiv \sigma_L/\sigma_T = \frac{1}{\varepsilon} \frac{r_{oo}^{o4}}{1-r_{oo}^{o4}}$$

Fig. 15a shows R versus $Q^2$ for different regions of W as determined by the DESY-Glasgow experiment.* $R(Q^2)$ rises linearly with $Q^2$ (for $Q^2 \leq 1.5$ GeV$^2$). Note that $\sigma_L$ and therefore R have to vanish at $Q^2 = 0$. The available data are well represented by the following parametrization:

$$R = \xi^2 \frac{Q^2}{m_\rho^2}$$

with $\xi^2$ being constant above W = 2 GeV and of the order of 0.5 (see Fig. 15b). This is close to the prediction of Fraas and Schildknecht[46], namely $R = Q^2/m_\rho^2$. The fact that $\xi^2 \neq 1$ could perhaps be ascribed to a difference in the total cross sections for longitudinal and transverse rho-nucleon scattering, $\xi = \sigma^{tot}_{\rho_L p}/\sigma^{tot}_{\rho_T p}$.[47]

## THE VDM CONTRIBUTION TO $\sigma_L^{tot}$

The measurement of $\xi$ provides an estimate of the VDM contribution to the total $\gamma_L p$ cross section $\sigma_L$ and a test of the hypothesis that $\sigma_L$ is described by VDM:

$$\sigma_L^{VDM} \approx \xi \frac{Q^2}{m_\rho^2} \frac{\sigma_T^{VDM}(Q^2 = 0)}{(1 + Q^2/M_\rho^2)^2}$$

Only one power of $\xi$ appears since $\sigma_L^{VDM}$ is related to the $\gamma_L p$ forward scattering amplitude. The quantity $\sigma_T^{VDM}$ denotes the sum of the $\rho,\omega,\Phi$ contributions to the total photon proton cross section, $\sigma_T^{VDM} \approx 0.86\sigma_{\gamma p}^{tot}$ (Ref. 48). The ratio $R = \sigma_L/\sigma_T$ can now be computed assuming $\sigma_L = \sigma_L^{VDM}$ and taking the measured data for $\sigma_T(Q^2)$. The comparison with experiment is shown in Fig. 16. The values predicted for R and hence for $\sigma_L$ are too large by a factor of 1.5 - 2.

---

* The R values calculated for W ≤ 2 GeV should be taken with caution since the assumption of SCHC is not satisfied at these low energies.

b) $\gamma_V p \to \omega p$

The data on ω production are less precise because the cross section is smaller. The energy dependence of the total cross section for photoproduction[42,45] at an average $Q^2$ of 0.7 $GeV^2$ (Ref. 49) is given in Fig.17. The electroproduction cross section near threshold is found to be large. The enhancement must be due to nonperipheral production of ω's since it is absent for events with $|t| < 0.5$ $GeV^2$. The same conclusion is reached from Fig. 18 which shows the ω cms production angular distribution in the threshold region. At higher W's (W > 2 GeV) the t distribution is more peaked forward (Fig. 19, Ref. 49). Surprisingly enough the $Q^2$ dependence of the large momentum transfer region ($|t| \geq 0.7$ $GeV^2$) is much weaker than for small $|t|$ values.

In Fig. 20 $\sigma_{\omega p}$ is shown as a function of $Q^2$ and compared to the VDM prediction. As in rho production $\sigma_{\omega p}$ exceeds the VDM cross section for small energies (1.7 < W < 2 GeV) but agrees with the VDM prediction at higher energies.

## 9. GLOBAL FEATURES OF ELECTROPODUCED FINAL STATES

Conventionally the data on multiplicities and single particle spectra are discussed assuming short range correlations and limited transverse momenta (Fig. 21). At high energies using the Feynman variable $x = p^*_{\parallel}/p^*_{max}$ ($p^*_{\parallel}, p^*_{max}$ = longitudinal and maximum possible momentum in the cms), the particles can be classified into those coming from beam fragmentation (x > 0), from target fragmentation (x < 0) and from the central region ($x \approx 0$). As a direct consequence of short range correlation we expect e.g. the pion distributions for $x \leq 0$ to be independent of $Q^2$. Likewise, since most pions are produced near x = 0, the multiplicity will not change drastically with $Q^2$. Note, however, that the particle classification is possible only at energies much higher (lns >> 4) than those covered by most experiments.

### a) CHARGED MULTIPLICITIES

The average number <n> of charged hadrons produced as a function of s is shown in Fig. 22 for different regions of $Q^2$. The electroproduction

points[36,50-52] follow the photoproduction result closely,

$$\langle n \rangle = 1 + \ln s.$$

The $Q^2$ behaviour of $\langle n \rangle$ for small and large $Q^2$ values is given in Fig. 23,24. For energies $W \lesssim 3$ GeV where $\langle n \rangle < 3$ at $Q^2 = 0$, the electroproduction values are lower by 8-10 % than the $Q^2 = 0$ point. The drop occurs at small $Q^2$ (below 0.3 GeV$^2$) and can be traced to two effects: the rapid disappearance of vector meson production which contributes to $n = 3$ final states, and the increasing importance of multineutral states with one charged hadron, $\gamma_V p \to p\pi^o\pi^o\ldots, \pi^+ n\pi^o\ldots$ (Ref. 51). At higher energies ($W > 3$ GeV) the multiplicity for $Q^2 > 0$ seems to exceed its photoproduction value slightly. Apart from these subtle points the multiplicity is remarkably constant with $Q^2$ and close to the $Q^2 = 0$ data. Note that the Cornell measurements (Fig. 24) reach well into the scaling region (for example, at $s = 9.6$ GeV$^2$ the highest $Q^2$ point has $\omega = 2.5$). Fig. 25 shows an interesting comparison of the relative yields of reactions with 1, 3, and 5 charge particles produced in electroproduction ($ep \to e'X$) (Ref 51) and in pp scattering ($pp \to p + X$) (Ref. 53). In both cases the system X has been analysed. The close agreement in shape (energy dependence) and magnitude is striking.

b) INCLUSIVE PION SPECTRA, $\gamma_V N \to \pi X$

All existing data agree that the pion yield normalized to the total cross section does not depend on $Q^2$ in the region $x \lesssim 0$. As an example, Fig. 26 shows the invariant normalized cross section,

$$F(x) = \frac{1}{\sigma_{tot}} \frac{1}{\pi} \int_0^{p_{\perp max}^2} \frac{E^*}{p^*_{max}} \frac{d\sigma}{dx dp_\perp^2} dp_\perp^2$$

for negative pions as a function of x. The open points stem from a photoproduction experiment (Ref. 54); the electroproduction data are averages over the $Q^2$ intervals 0.3 to 0.5 GeV$^2$ and 0.5 to 1.4 GeV$^2$ (Ref. 51). For $x < 0$ no significant change with $Q^2$ is observed. A high statistics experiment done by a Harvard-Cornell collaboration[55] on $\pi^+$ emitted at $x = 0$ did not find any $Q^2$ dependence either. The experiment was done at

W = 2.65 GeV for $Q^2$ = 1.2 $GeV^2$ ($\omega$ = 6), 2 $GeV^2$ ($\omega$ = 4) and 3.6 $GeV^2$ ($\omega$ = 2.7) and covered the full range of transverse momenta (Fig. 27).

A strong variation with $Q^2$ is observed in the photon fragmentation region ($x > 0$); e.g. the yield of forward produced $\pi^-$ is reduced by a factor of 2-4 between $Q^2 = 0$ and $Q^2 \approx 0.5$ $GeV^2$ (see Fig. 26). To a large extent this reduction can be ascribed to the $Q^2$ behaviour of $\rho^o$ production, $\gamma_V p \to \rho^o p$, which at $Q^2 = 0$ is the major source of forward $\pi^-$ production. Removal of the $\rho^o$ events reduces the difference between photo and electroproduction data (see Fig. 26).

c) CHARGE RATIOS

Previous measurements of charge ratios indicated in the photon fragmentation region a rapid rise with $Q^2$ of positive over negative hadron yields for proton targets (see Ref. 2). This observation was taken as a further evidence in favor of the quark-parton picture where a charge asymmetry of the observed type comes out quite naturally: the photon interacts with a quark $q_i$ of type i (see Fig. 28). The struck quark recombines with a quark $\bar{q}_j$ from the quark sea to form a meson M. The cross section is of the form

$$\sigma_{\gamma_V p \to (q_i \bar{q}_j)X} \sim N_i \text{ (charge of } q_i)^2$$

where $N_i$ = number of quarks of type i inside the proton.
Considering only valence quarks and the pseudoscalar nonet leads to the following particle ratios:

| | $\pi^+$ | $\pi^-$ | $K^+$ | $K^-$ | $K^o$ | $\bar{K}^o$ |
|---|---|---|---|---|---|---|
| $\gamma p$: | 8 | 1 | 8 | 0 | 1 | 0 |
| $\gamma n$: | 4 | 2 | 4 | 0 | 2 | 0 |

For a proton target the $\pi^+/\pi^-$ ratio, which experimentally is ~1.2 at $Q^2 = 0$ will increase to 8 and the $K^+/\pi^+$ ratio will approach unity in this simple minded picture. Production of other meson resonances and the inclusion of distribution functions for u and d quarks will lower the predicted ratios.

New infromation on particle ratios comes from the Harvard group[56], from the SLAC-MIT[57] and the UCSC-SLAC experiments[36]. In the first experiment the charge ratio has been measured for pions while the latter two have determined only the ratio of positive to negative hadron yields. Fig. 29 shows the $\pi^+/\pi^-$ ratio as a function of x for pions produced at small transverse momenta ($p_\perp^2 < 0.02$ GeV$^2$). As expected, the charge ratio is close to one at x = 0; it reaches a maximum value of two around x = 0.5 and approaches unity as $x \to 1$. Hence the excess of $\pi^+$ over $\pi^-$ is not due to low mass two body channels such as $\gamma_V p \to \pi^+ n$ which would show up near x = 1. The $h^+/h^-$ ratio measured in the SLAC-MIT experiment for $0.4 < x < 0.85$ is displayed in Fig. 30. The experiment covers a wide range of energies ($11 < s < 31$ GeV$^2$). At all energies the $h^+/h^-$ ratio increases with $Q^2$ and for fixed $\omega$ it appears to be independent of s, i.e. it scales. Fig. 31 summarized the $\pi^+/\pi^-$ ratios ($R_\pi$) and the $h^+/h^-$ ratios ($R_h$) as a function of $\omega$. Both quantities rise with decreasing $\omega$: the $\pi^+/\pi^-$ ratio rises from 1.2 at $\omega = \infty$ ($Q^2 = 0$) to ~2 at $\omega = 2$; the $h^+/h^-$ ratio, which is significantly larger rises from 1.5 at $\omega = 100$ to ~3 at $\omega = 3$.

The larger value of $R_h$ is caused mainly by additional contributions from $K^+$ and p production. We have used the data from Refs. 52, 56, 58 and 59 to estimate

$$R_h = \frac{N_{\pi^+} + N_{K^+} + N_p}{N_{\pi^-} + N_{K^-} + N_{\bar{p}}}$$

at $\omega = 4.2$ and $0.4 < x < 0.85$. We find $N_{K^+} \approx 0.3 N_{\pi^+}$, $N_p \approx 0.1 N_{\pi^+}$*, $N_{K^-} \lesssim 0.1 N_{\pi^-}$, $N_{\bar{p}} \approx 0$ and hence $R_h \approx 1.3\, R_\pi$ in fair agreement with Fig.31. The charge ratios on a neutron target are given in Fig. 32. The $\omega$ dependence is small; $R_\pi$ and $R_h$ lie between 1.0 and 1.3. The curves in Figs. 31, 32 show the result of a quark model claculation[61] which used the proton data on $R_h$ (assuming $R_h = R_\pi$) to predict the neutron target. A new fit

---

* The proton contribution is actually larger[60]. For protons with a given x a larger x value will be calculated when a proton is mistakenly treated as a pion. This is because the wrong mass is used for the Lorentz transformation into the cms. For example, for s = 13 GeV$^2$, $Q^2$ = 1.5 GeV$^2$ a proton with $p_\perp = 0$, $x_p = 0.2$ treated as a pion will give $x_\pi = 0.45$. Taking this effect into account increases $N_p$ to $\approx 0.2\, N_\pi$.

starting from the measured $R_\pi$ values will probably improve the agreement.

While the observed charge ratios are - at least qualitatively - in agreement with the quark parton picture they can also be described e.g. in a Regge model[62].

d) $K^+$ PRODUCTION

The increase of $K^+$ relative to $\pi^+$ production with $Q^2$ is quite spectacular and in line with the simple quark picture described above. This increase was first seen in an experiment at DESY[59]. Fig. 33 shows the recent results of the Harvard group[63a]. While the $K^+/\pi^+$ ratio at $Q^2 = 0$ and $x \geq 0.3$ is around 0.1 (Ref. 63b) it has grown to 0.3 - 0.4 for $Q^2 \geq 1$ GeV$^2$ (The line in Fig. 33 indicates the $\pi^+$ yield multiplied by 0.2). The rise is observed for $x \geq 0.3$, i.e. it cannot be considered confined to the $x \approx 1$ region. It is therefore not solely due to low mass two body states such as $\gamma_V p \to K^+\Lambda$ and $K^+Y(1385)$. Qualitatively, the observed increase agrees with K. Wilson's prediction[64] $K^+/\pi^+ \to 1$ a $Q^2 \to \infty$ .

e) $Q^2$ DEPENDENCE OF $p_\perp$ DISTRIBUTIONS

The DESY-Glasgow collaboration has measured the average $\langle p_\perp^2 \rangle$ for $\pi^-$ production, $\gamma_V p \to \pi^- X$, as a function of x.[51] The result is shown in Fig. 34 for three different W intervals (1.5 - 1.8 GeV, 1.8 - 2.2 GeV, 2.2 - 2.8 GeV). Note that kinematics forces $p_\perp \to 0$ as $|x| \to 1$. A noticeable increase in $\langle p_\perp^2 \rangle$ due to phase space is observed from the first to the second W interval. In the highest W interval a behaviour similar to purely hadronic reactions is seen: $\langle p_\perp^2 \rangle$ has a minimum at x = 0 and increases towards positive and negative x values. For x values between 0.4 and 0.8 the average transverse momentum is significantly larger than at $Q^2 = 0$. Fig. 35 shows $\langle p_\perp^2 \rangle$ versus $Q^2$ in the photon fragmentation region using data from DESY-Glasgow, SLAC-MIT and UCSC-SLAC.
Both sets of data show a similar trend: the average $p_\perp$ rises rapidly between $Q^2 = 0$ and 1 GeV$^2$ and appears to level off at higher $Q^2$ values.

A broadening of the $p_\perp$ distribution has also been observed for inclusive $\pi^0$ production. In Fig. 36 the slope of the $p_\perp^2$ distribution for

inclusive $\pi^+$ and $\pi^o$ production is given as a function of $Q^2$. The $\pi^+$ points come from SLAC (Ref. 65), the $\pi^o$ data from the UC-Santa Barbara group at SLAC[66].

Theoretically a rising $\langle p_\perp^2 \rangle$ in the photon fragmentation region is not unexpected. In fact, it would have been rather surprising to find the opposite, for a variety of reasons: $t_{min}$ effects tend to increase $\langle p_\perp^2 \rangle$ (see section 4); the wave length of the virtual photon becomes smaller with increasing $Q^2$ and the scattering presumably less peripheral. This was shown to be true in models where the photon scatters off virtual particles (with form factors)[67,68]. In these models $\langle p_\perp^2 \rangle$ is predicted to increase without limit as $Q^2 \to \infty$. A different behaviour is obtained in models in which the photon has two components, one coupled directly to vector mesons and a socalled bare on which couples only to the charge of the pointlike constituents (partons). Proceeding from photoproduction to the deep inelastic region the hadron component becomes less important and $\langle p_\perp^2 \rangle$ increases. However, parton models require a $p_\perp$ cutoff which does not depend on $Q^2$ in order to produce scaling[68]. Therefore, they predict that $\langle p_\perp^2 \rangle$ becomes independent of $Q^2$ as $Q^2 \to \infty$. Clearly, the present data do not permit a decision on whether $\langle p_\perp^2 \rangle$ keeps on growing or becomes constant with increasing $Q^2$.

## 10. CONCLUDING REMARKS

The data presented to this conference indicate that the photon-nucleon interaction becomes less peripheral as $Q^2$ grows. Evidence for this can be found in the behaviour of

(a) the two-body channels $\gamma_V p \to \pi^+ n$ and $\gamma_V p \to \omega p$, where $d\sigma/dt$ for $|t| > 1$ GeV$^2$ is seen to have a much weaker falloff with $Q^2$ than for small momentum transfers;

(b) the inclusive pion production which shows a broadening of the $p_\perp$ distribution with increasing $Q^2$.

The small t data on $\rho$ and $\omega$ production for energies above 2 GeV agree well with the vector dominance predictions.

The next step necessary is a study of higher vector meson states such as the $\rho(1500)$. Such data would test the extended version of VDM which

includes higher vector mesons[69] and off-diagonal scattering terms[70], and which is able to fit the total cross section data[71]. If off-diagonal terms are important (in particular $\rho(770)p \to \rho(1500)p$) the $Q^2$ dependence of $\sigma(\gamma_V p \to \rho(1500)p)$ will not be given by a simple $\rho(1500)$ pole formula. At Cornell two experiments are in preparation which can answer this question. One is a streamer chamber experiment done in collaboration with DESY; the other is called LAME and uses a set of proportional chambers inside a magnet. Fig. 37 shows one of the first multihadron events observed with LAME.

ACKNOWLEDGEMENTS

Discussions with Drs. K. Hanson, D. Kreinick, H. Meyer, D. Schildknecht and T. Walsh have been very helpful. The author wants to thank Profs. J. Ballam and W.K.H. Panofsky for the kind hospitality extended to him at SLAC. He is grateful to Mrs. E. Hell for her help with the manuscript.

List of References


1. G. Weber, DESY Report 75/17 (1975) and EPS International Conference on High Energy Physics, Palermo, Italy, 23-28 June, 1975;
G. Moorhouse, ibid. and Glasgow University preprint.
C.A. Heusch, ibid.

2. K. Hanson, Rapporteur Talk at this conference.
R. Mozley, ibid.
L. Mo, ibid.

3. K. Berkelman, Proceedings of the XVI International Conference on High Energy Physics, Chicago, 1972, ed. by J.D. Jackson and A. Roberts, Vol.4, p.41;
F.W. Brasse, 1973 International Symposium on Lepton and Photon Interactions at High Energies, Bonn, ed. by H. Rollnik and W. Pfeil, p. 251;
A.B. Clegg, ibid., p. 49;
H. Meyer, ibid., p. 175;
K.C. Moffeit, ibid., p. 313;
R. Talman, ibid., p. 145;
P. Söding, Lectures at the III Winter Meeting on Fundamental Physics, Sierra Nevada (Spain), Feb. 1975, ed. by J. Diaz-Bejerano, p.61;
J.D. Sullivan, Talk presented at the Conference of Recent Advances in Particle Physics, March 15-17, 1973, Univ. of Illinois preprint Ill-(TA)-73-2;
F.J. Gilman, SLAC-PUB-1396 (1974).

4. E. Evangelides et al., Nucl. Phys. B71, 381 (1974).

5. J.-C. Alder et al., DESY Report 75/29 (1975) and paper contributed to this conference.

6. J. Gayler, DESY Report, Lecture presented at the VIII All Soviet Union High Energy Physics School, Erevan, April 1975.

7. see e.g. R.C.E. Devenish and D.H. Lyth, DESY Report 75/4 (1975);
A. Donnachie, Rapporteur Talk at this conference.

8. P. Brauel et al., contribution to this conference.

9. C.J. Bebek et al., contribution to this conference.

10. F.A. Berends and R. Gastmans, Phys. Rev. D5, 205 (1972);
R.C.E. Devenish and D.H. Lyth, Phys. Rev. D5, 47 (1972);
P.W. Manweiler and W. Schmidt, Phys. Rev. D3, 2752 (1971);
W. Schmidt, DESY Report 71/22 (1971);
F. Gutbrod and G. Kramer, Nucl. Phys. B49, 461 (1972);
For a review see M. Gourdin, Physics Reports 11C, 29 (1974).

11. (a) G.Adylov et al., Dubna Report JIRN, E1-8047 (1974), paper submitted to the XVII International Conference on High Energy Physics, London, July 1-10, 1974.

(b) S.F. Berezhnev et al., Nucl. Phys. 16, 99 (1973).

12. see e.g. K.C. Moffeit, Rapporteur Talk at the 1973 International Symposium on Electron and Photon Interactions at High Energies, Bonn, Aug. 27-31, 1974, p.313.

13. B. Hyams et al., CERN preprint (1975).

14. A. Actor, I. Bender and J.G. Körner, Nuovo Cimento 24A, 369 (1974).

15. F.W. Brasse et al., DESY Report 75/23 (1975).

16. G. Kramer, Acta Physica Austrica 40, 150 (1974).

17. H. Harari, Proceedings of the 1971 International Symposium on Electron and Photon Interactions at High Energies, Cornell, ed. by N.B. Mistry, p. 299.

18. G. Moorhouse (see Ref. 1) has suggested that a rapid switch from dominant s-channel helicity 3/2, $A_{3/2}$ to dominant $A_{1/2}$, is responsible for the disappearance of the second maximum. A. Donnachie (private communication) has argued that the interference of $J_1(R\sqrt{-t})$ and a cut contribution which rapidly increases with $Q^2$ is responsible.

19. T. Azemoon et al., DESY Report 74/45 (1974).

20. C.N. Brown et al., Phys. Rev. Letters 28, 1682 (1972).

21. C.J. Bebek et al., Phys. Rev. Letters 32, 21 (1974) and C.J. Bebek et al., Harvard preprint, contribution to this conference.

22. see e.g. the compilation of coupling constants, G. Ebel et al., Springer Tracts in Modern Physics, Vol. 55, 239 (1970).

23. A. Bartl and W. Majerotto, Nucl. Phys. B90, 285 (1975).

24. P. Joos et al., Phys. Letters 52B, 481 (1974) and contribution to this conference.

25. P. Stichel and M. Scholz, Nuovo Cimento 34, 1381 (1964).

26. D. Lüke and P. Söding, Springer Tracts in Modern Physics 59, 39 (1971).

27. F.A. Berends and R. Gastmans, Phys. Rev. D5, 204 (1972).

28. P. Levi and W. Schmidt, contribution to this conference.

29. A. Bartl, W. Majerotto, and D. Schildknecht, Nuovo Cimento 12A, 703 (1972).

30. K. Wacker and P. Söding, private communication.

31. D.T. Botterill et al., Phys. Letters 45B, 405 (1983); for updated results see Ref. 1.

32. E. Amaldi et al., Phys. Letters 41B, 216 (1972).

33. P. Brauel et al., Phys. Letters 45B, 389 (1973).

34. Prof. Perkins, Rapporteur Talk given at this conference.

35. DESY-Glasgow Collaboration, contribution to this conference.

36. UCSC-SLAC collaboration, contribution to this conference.

37. J. Dakin et al., Phys. Rev. D8, 687 (1973).

38. L. Ahrens et al., Phys. Rev. Letters 31, 131 (1973); Phys. Rev. D9, 1894 (1974).

39. Y.F. Pirogov, N.L. Ter-Isaakian, Yerevan preprint, contribution to this conference.

40. G. Preparata, Phys. Letters 49B, 374 (1974).

41. For a discussion of a shrinking photon see e.g. J.D. Bjorken, J. Kogut and D. Soper, Phys. Rev. D1, 1382 (1971); H.T. Nieh, Phys. Letters B38, 100 (1972).

42. SLAC-Berkeley-Tufts Collaboration, Phys. Rev. D5, 545 (1972); D7, 3170 (1973); Weizmann-SLAC-Tel Aviv Collaboration, Phys. Rev. D5, 131 (1973); F. Bulos et al., Data quoted by D.W.G.S. Leith in Lectures presented to the Scottish Universities Summer School in Physics (1970).

43. J. Ballam et al., Phys. Rev. D10, 765 (1974).

44. K. Schilling and G. Wolf, Nucl. Phys. B61, 381 (1973).

45. Aachen-Berlin-Bonn-Hamburg-Heidelberg-München Collaboration, Phys. Rev. 175, 1669 (1968).

46. H. Fraas and D. Schildknecht, Nucl. Phys. B14, 543 (1969).

47. The nature of the parameter $\xi$ may be decided by measuring rho electroproduction on nuclei; see e.g. S.R. Gevorkyan and V.M. Zhamkochyan, Yerevan preprint, contribution to this conference.

48. see e.g. G. Wolf, Proceedings of the 1971 International Symposium on Electron and Photon Interactions at High Energies, Cornell, ed. by N.B. Mistry, p. 189; and DESY Report 72/61 (1972).

49. DESY-Glasgow Collaboration, contribution to this conference.

50. J. Ballam et al., Phys. Letters 56B, 193 (1975).

51. DESY-Glasgow Collaboration, contribution to this conference.

52. P.H. Gabrincius et al., Phys. Rev. Letters 32, 328 (1974);
A.J. Sadoff et al., Phys. Rev. Letters 32, 955 (1974).

53. The pp data come from a bubble chamber experiment of the Bonn-Hamburg-DESY-Munich Collaboration; see B. Schwarz (Ph.D. thesis), DESY internal report F1-74/7 (1974).

54. Aachen-Hamburg-Heidelberg-Munich Collaboration, data quoted by Ref. 51.

55. S.D. Holmes et al., contribution to this conference.

56. C.J. Bebek et al., Harvard University preprint.

57. SLAC-MIT Collaboration, data presented to this conference.

58. I. Dammann et al., DESY Report 72/70 (1972); Nucl. Phys. B54, 381 (1973).

59. J.C. Alder et al., Nucl. Phys. B46, 415 (1972).

60. H. Meyer, private communication.

61. J.T. Dakin and J.G. Feldman, Phys. Rev. D8, 2862 (1973).

62. W-S. Lam, J. Tran Thanh Van, I. Ushersohn, Nucl. Phys. B74, 59 (1974).

63. (a) C.J. Bebek et al., contribution to this conference.
(b) H. Burfeindt et al., Nucl. Phys. B74, 189 (1974).

64. K. Wilson, Triese preprint, IC/71/47 (1971).

65. J.T. Dakin et al., Phys. Rev. D10, 1401 (1974).

66. D.O. Caldwell et al., Contribution to this conference.

67. F. Gutbrod and U.E. Schröder, Nucl. Phys. B62, 381 (1973).

68. see e.g. S.D. Drell, D.J. Levy and T.-M. Yan, Phys. Rev. 187, 2159 (1969); D1, 1035, 2402 (1970).

69. J.J. Sakurai and D. Schildknecht, Phys. Letters 40B, 121 (1972); 41B, 489 (1972); 42B, 216 (1972).
A. Bramon, E. Etim and M. Greco, Phys. Letters 41B, 609 (1972); M. Greco, Nucl. Phys. B63, 398 (1973).

70. D. Schildknecht, DESY Report 74/39 (1974);
H. Fraas, B.J. Read and D. Schildknecht, Nucl. Phys. B86, 346 (1975).

71. R. Devenish and D. Schildknecht, DESY Report 75/18 (1975).

FIGURE CAPTIONS

1. Forward cross section for $\gamma_V p \to \pi^+ n$ at $Q^2 = 0.4$ GeV$^2$ (Ref.4) and $Q^2 = 0.6$ and 1 GeV$^2$ (Ref. 5).

2. Cms angular distributions for $\gamma_V p \to \pi^+ n$ in the regions of the 2$^{nd}$ and 3$^{rd}$ resonances for $Q^2 = 0.6$ and 1 GeV$^2$ (Ref. 5).

3. Differential cross section $d\sigma/dt$ for $\gamma_V p \to \pi^+ n$ at W = 2.2 GeV for different values of $Q^2$ from DESY (Ref. 8) and Harvard (Ref. 9). The curve indicates the photoproduction result.

4. The cross section ratio $(\gamma_V d \to \pi^+ n n_s)/(\gamma_V d \to \pi^- p p_s)$ at $Q^2 = 0$ and 0.7 GeV$^2$ (Ref. 8).

5. The pion form factor $F_\pi(Q^2)$ multiplied by $Q^2$. The data were taken from Ref. 9.

6. The reaction $\gamma_V p \to \pi^o p$: the cross section $\frac{2}{1+\varepsilon} 2\pi \frac{d^2\sigma}{dt d\Phi}$ versus t for different values of $Q^2$ (Ref. 15).

7. The reaction $\gamma_V p \to \pi^o p$: the cross section $\frac{2}{1+\varepsilon} 2\pi \frac{d^2\sigma}{dt d\Phi}$ versus $Q^2$ for different values of t. Data taken from Ref. 15.

8. The differential cross section $\frac{d\sigma}{dt}$ for $\gamma_V p \to K^+ \Lambda$ and $\gamma_V p \to K^+ \Sigma^o$ as a function of $Q^2$. Only data with W = 2.2 GeV and $0.1 < |t| < 0.18$ GeV$^2$ were selected. The DESY data are those of Ref. 19. The CEA data come from Ref. 20.

9. The total cross section for $\gamma_V p \to \pi^- \Delta^{++}$ as a function of W averaged over the $Q^2$ interval 0.3 - 1.4 GeV$^2$ (Ref. 24).

10. (a) The total cross section for $\gamma_V p \to \pi^- \Delta^{++}$ as a function of $Q^2$ in the threshold region ($1.3 < W < 1.5$ GeV).

10. (b) The axial vector form factor as a function of $Q^2$.
Figure taken from Ref. 24.

11. Reaction $\gamma_V p \to p\pi^+\pi^-$: The $\pi^+\pi^-$ mass distribution. Shaded events have $|t| < 0.5$ GeV$^2$ (Ref. 35).

12. Reaction $\gamma_V p \to \rho^o p$: The ratio of $\sigma_\rho(Q^2)/\sigma_\rho(0)$ versus $Q^2$. The data have been taken from Refs. 35-38. The solid curves show the VDM prediction.

13. The slope parameter $A_{\rho p}$ defined by $\frac{d\sigma}{dt} \propto \exp(A_{\rho p} t)$ for $\rho$ production as a function of $\Delta\tau$. The data have been taken from Refs. 35-37,42,43.

14. Reaction $\gamma_V p \to \rho^o p$.
(a) The W dependence of the $\rho$ spin density matrix element $r^{o4}_{oo}$ versus W at $Q^2 = 0$ (Ref. 45) and for $0.3 < Q^2 < 1.4$ GeV$^2$ (⧫ Ref. 35, + Ref. 43).

(b) The phase between the longitudinal and transverse photon rho production amplitudes. (⧫ Ref. 35, + Ref. 43, ✳ Ref. 37).

15. Reaction $\gamma_V p \to \rho^o p$.

(a) The ratio $R = \sigma_L/\sigma_T$ versus $Q^2$ for different values of W (Ref. 35).
(b) The parameter $\xi^2 = R/(Q^2/m_\rho^2)$ versus W (⧫ Ref. 35, ⧫ Ref. 36, + Ref. 43, ✳ Ref. 37).

16. The ratio $R = \sigma_L/\sigma_T$ for the total photon proton cross section compared with the VDM prediction (curve, see text). The data come from a SLAC-MIT experiment.

17. Cross section for $\gamma_V p \to \omega p$ as a function of W. The $Q^2 = 0$ points stem from Refs. 42,45. The electroproduction measurements come from Ref. 49.

18. Reaction $\gamma_V p \to \omega p$. Differential cross section $\frac{d\sigma}{d\Omega}$ in the cms for the threshold region $1.7 < W < 2.0$ GeV for $0.3 < Q^2 < 1.4$ GeV$^2$ (Ref.49).

19. Reaction $\gamma_V p \to \omega p$: $d\sigma/dt$ versus $|t|$ at $Q^2 = 0$ (Refs. 42,45) and $0.3 < Q^2 < 1.4$ GeV$^2$ (Ref. 49).

20. Reaction $\gamma_V p \to \omega p$: The ratio of $\sigma_\omega(Q^2)/\sigma_\omega(0)$ versus $Q^2$. The data have been taken from Refs. 36 and 49. The solid curves show the VDM prediction.

21. Illustration of particle production in $\gamma_V p$ collisions at high energies.

22. Average charged multiplicity vs $s$ for different $Q^2$ intervals. Data come from Refs. 36, 50-52.

23. Average charged multiplicity vs $Q^2$ (Ref. 51).

24. Average charged multiplicity vs $Q^2$ (Ref. 52).

25. Fractional prong cross sections as a function of $s$ for electroproduction (data points, Ref. 51) and for $pp \to pX$ (Ref. 53) where $s$ is the square of the mass of X and the number of charged particles is that of the system X.

26. The invariant cross section for inclusive $\pi^-$ production, $\gamma_V p \to \pi^- X$, as a function of x at $Q^2 = 0$ for all data with a $\rho$ cut (in this case the data have been renormalized to $\sigma_{tot} - \sigma_\rho$) for the $Q^2$ intervals 0.3 - 0.5 and 0.5 - 1.4 $GeV^2$ (Ref. 51).

27. The invariant cross section for inclusive $\pi^+$ production, $\gamma_V p \to \pi^+ X$, at $x \simeq 0$ as a function of $x_T = p_T/p^*_{max}$.

28. Photon nucleon scattering in a quark model.

29. The $\pi^+/\pi^-$ ratio for inclusive $\pi$ production versus X at W = 2.1 GeV for $p^2 < 0.02$ $GeV^2$ (Ref. 56).

30. The ratio of positive to negative hadron production for $0.4 < x < 0.85$ as a function of s:
(a) for fixed $Q^2$
(b) for fixed $\omega$.
Data taken from Ref. 57.

31. The charge ratio for $\gamma_V p \to \pi^\pm X$, $h^\pm X$ versus $\omega$. (Refs. 56,57,58). The curve represents the calculation of Dakin and Feldman (Ref. 61).

32. The charge ratio for $\gamma_V n \to \pi^\pm X$, $h^\pm X$ versus $\omega$. (Refs. 56,57). The curve represents the prediction of Dakin and Feldman (Ref. 61).

33. The invariant cross section for inclusive $K^+$ production, $\gamma_V p \to K^+ X$, versus x. The solid line represents the invariant cross section for $\pi^+$ production multiplied by 0.2 (Ref. 63a).

34. Inclusive $\pi^-$ production, $\gamma_V p \to \pi^- X$; $\langle p^2 \rangle$ versus x for different W and $Q^2$ intervals (Ref. 51).

35. Inclusive $\pi$ production, $\gamma_V p \to \pi X$; $\langle p_\perp^2 \rangle$ versus $Q^2$ for $2.2 < W < 2.8$ GeV (Ref. 51) and $12 < s < 30$ $GeV^2$ (Ref. 64).

36. Slope of the $p_\perp^2$ distribution for $\gamma_V p \to \pi^+ X$ (Ref. 65) and $\gamma_V p \to \pi^o X$ (Ref. 66) versus $Q^2$.

37. Computer display of a multiprong event of the type $ep \to e'X$ observed with LAME. The beam enters the magnet from the left. The skewed lines mark the position of the proportional chambers. The curved lines show the reconstructed tracks. The positions of water Cerenkov counters (at top and bottom) and shower counters (to the right) are also marked. (Private communication by H. White.)

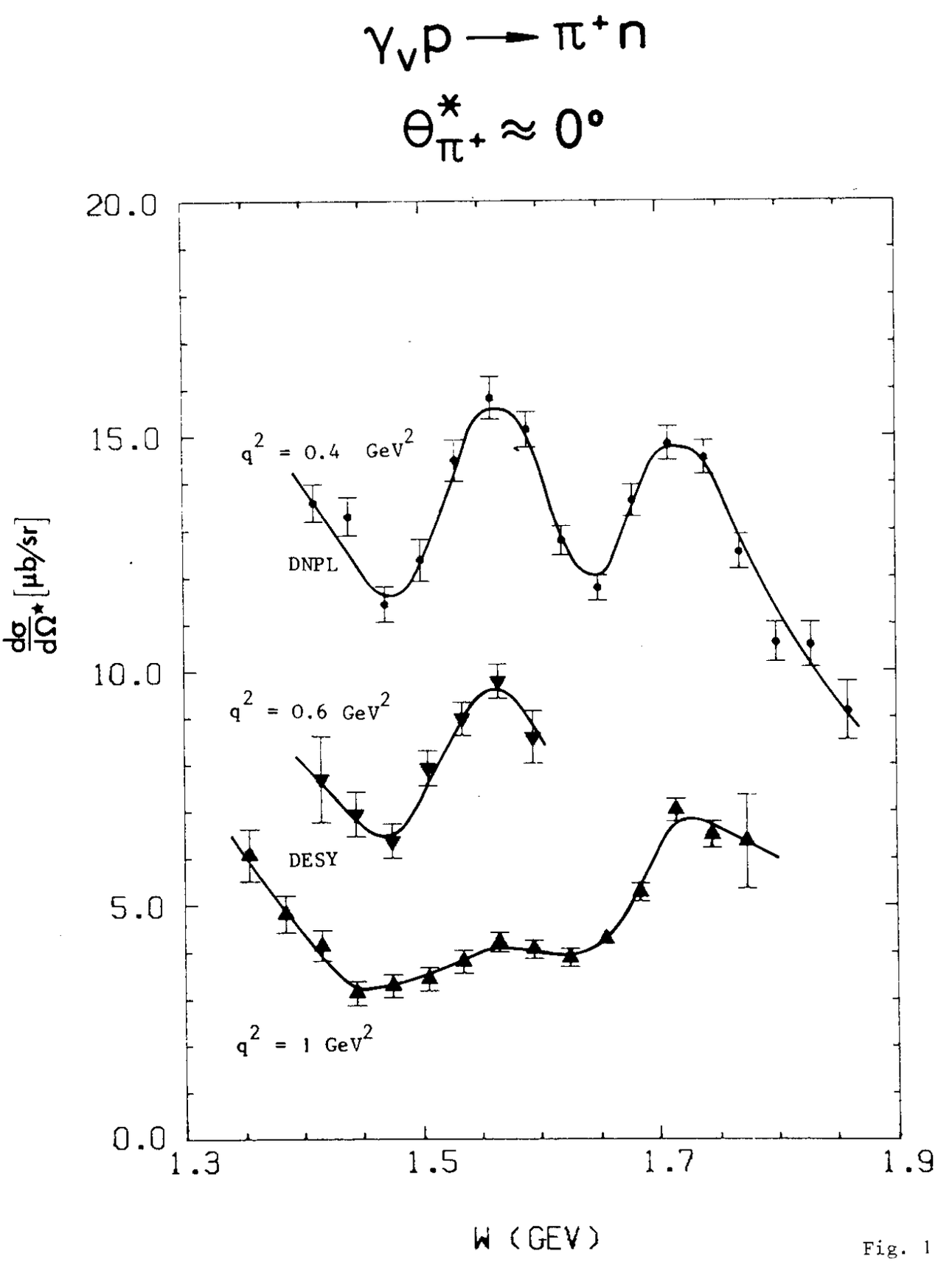
$\gamma_v p \longrightarrow \pi^+ n$
$\theta^*_{\pi^+} \approx 0°$
20.0
15.0
10.0
5.0
0.0
1.3
1.5
1.7
1.9
$\frac{d\sigma}{d\Omega^*}$ [μb/sr]
W (GEV)
$q^2$ = 0.4 GeV$^2$
DNPL
$q^2$ = 0.6 GeV$^2$
DESY
$q^2$ = 1 GeV$^2$

Fig. 1

$\gamma_v p \rightarrow \pi^+ n$

$q^2 = 1\ GeV^2$

DESY

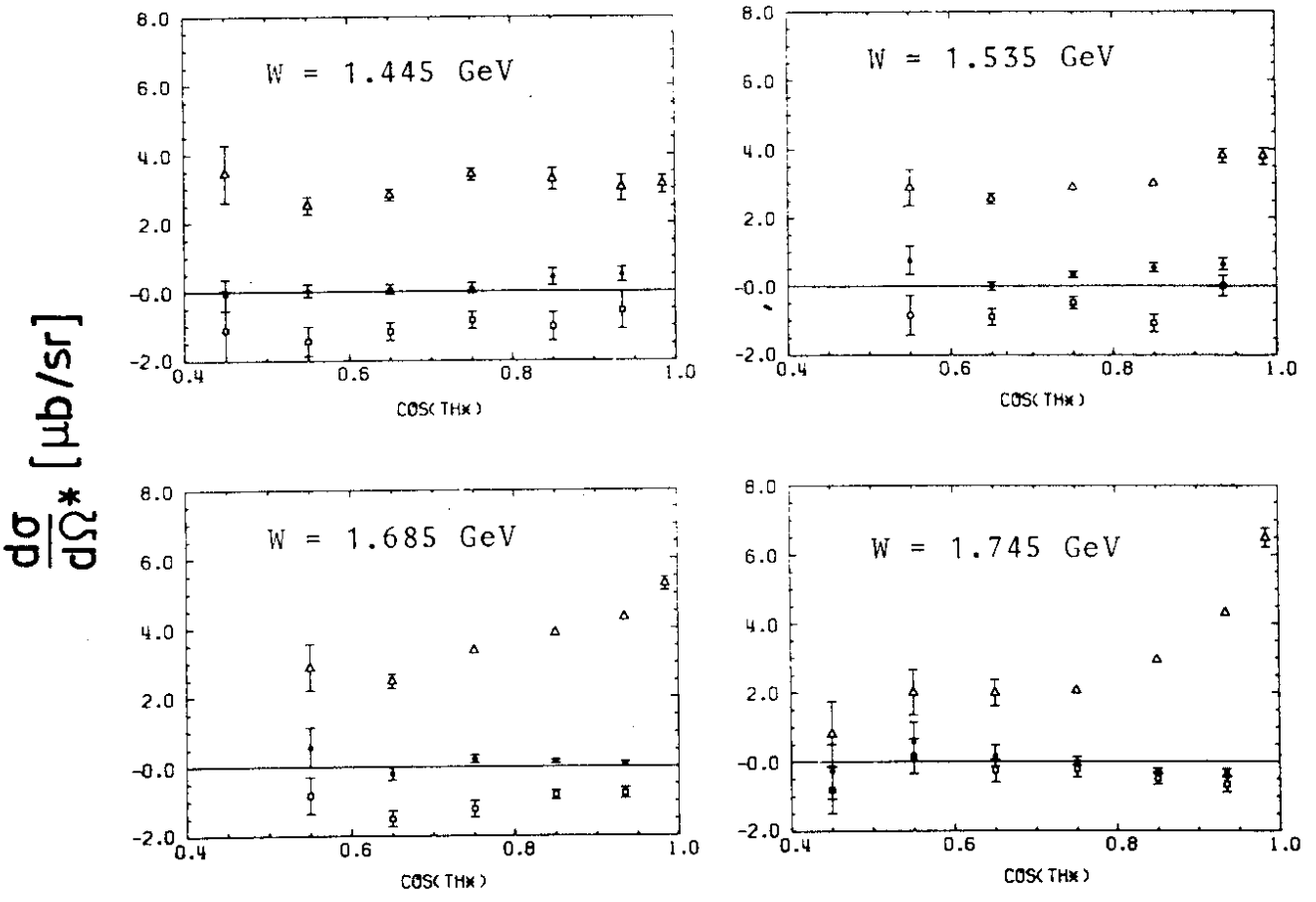


$\Delta\ \sigma_U + \varepsilon\sigma_L$ , $\square\ \sigma_P$ , $o\ \sigma_I$

Fig. 2

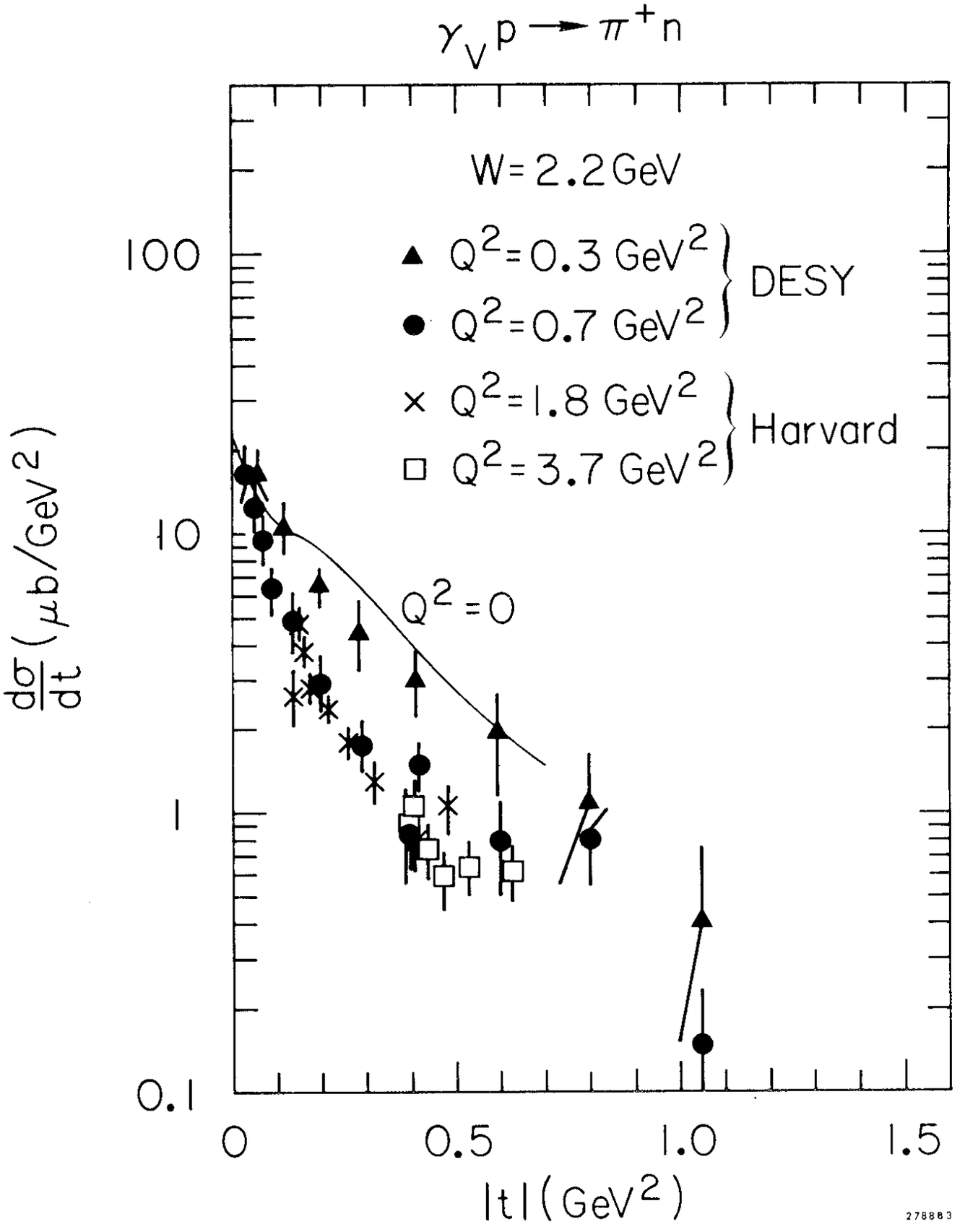
$\gamma_V p \rightarrow \pi^+ n$
W = 2.2 GeV
$Q^2 = 0.3$ GeV$^2$
$Q^2 = 0.7$ GeV$^2$
DESY
$Q^2 = 1.8$ GeV$^2$
$Q^2 = 3.7$ GeV$^2$
Harvard
$Q^2 = 0$
$\frac{d\sigma}{dt}$ ($\mu$b/GeV$^2$)
100
10
1
0.1
0
0.5
1.0
1.5
$|t|$ (GeV$^2$)
278883

Fig. 3

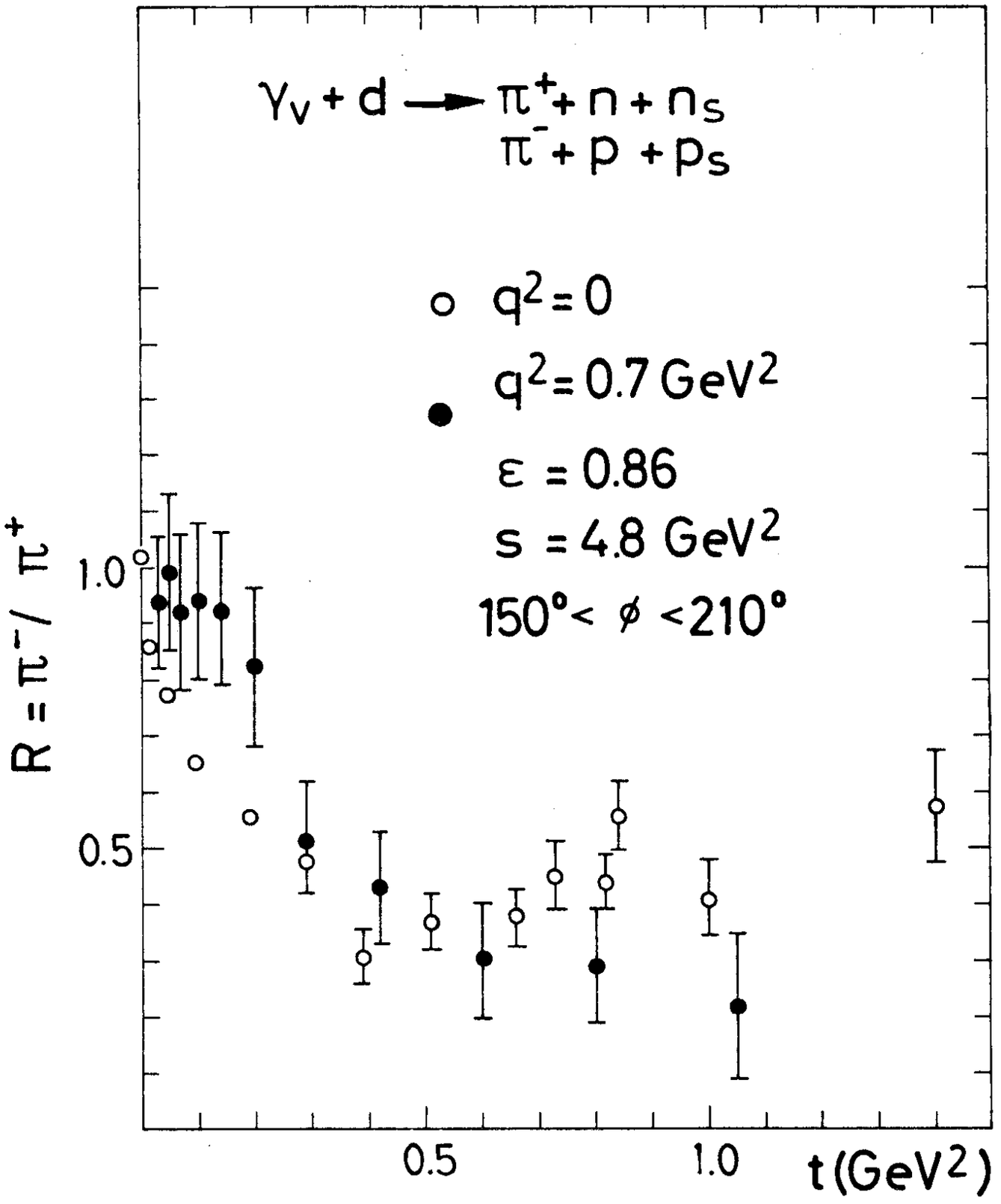
$\gamma_V + d \rightarrow \pi^+ + n + n_s$
$\pi^- + p + p_s$
$q^2 = 0$
$q^2 = 0.7\ GeV^2$
$\varepsilon = 0.86$
$s = 4.8\ GeV^2$
$150° < \phi < 210°$
$R = \pi^- / \pi^+$
1.0
0.5
0.5
1.0
$t(GeV^2)$

Fig. 4

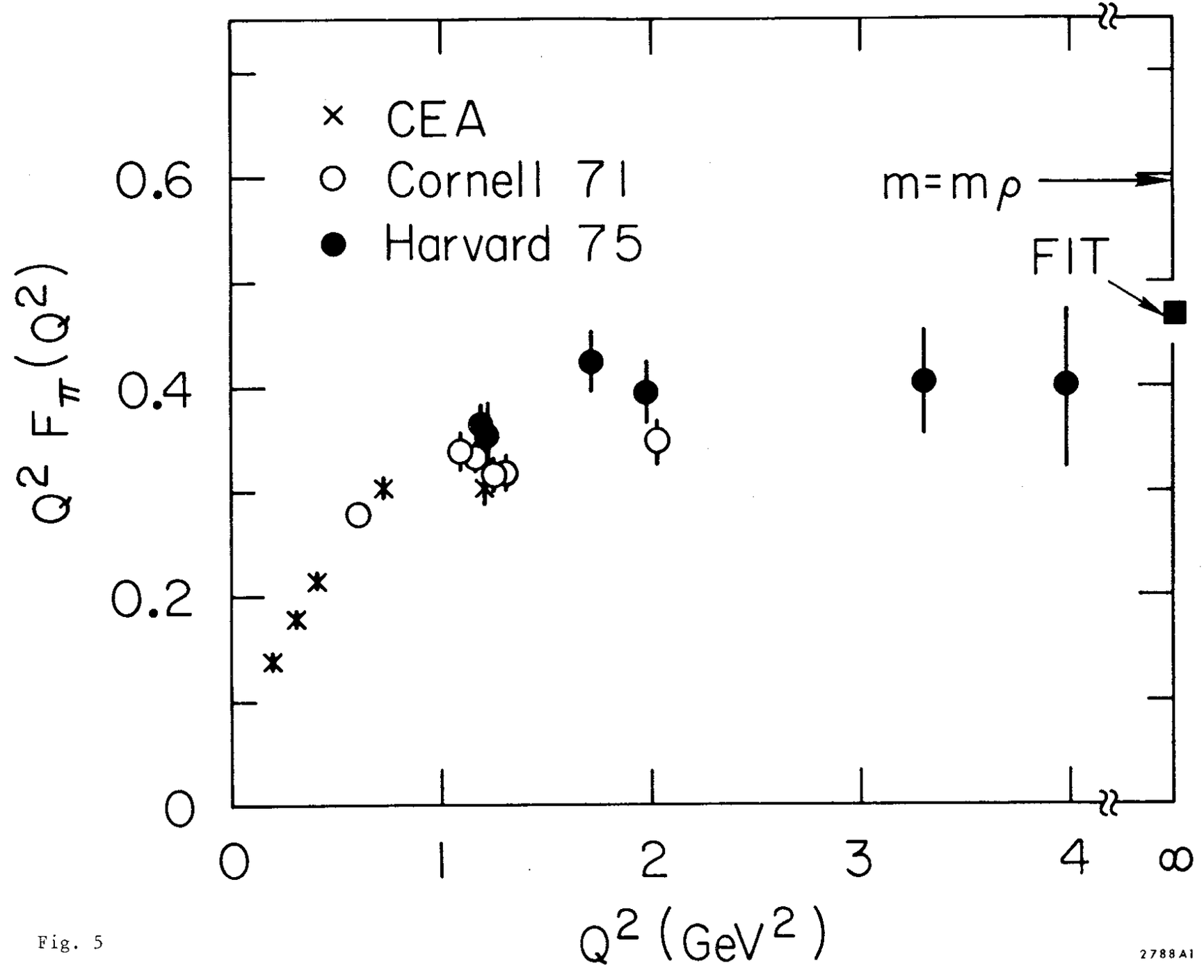
CEA
Cornell 71
Harvard 75
m=mρ
FIT
$Q^2 F_\pi(Q^2)$
0.6
0.4
0.2
0
0
1
2
3
4
∞
$Q^2$ (GeV$^2$)
2788A1

Fig. 5

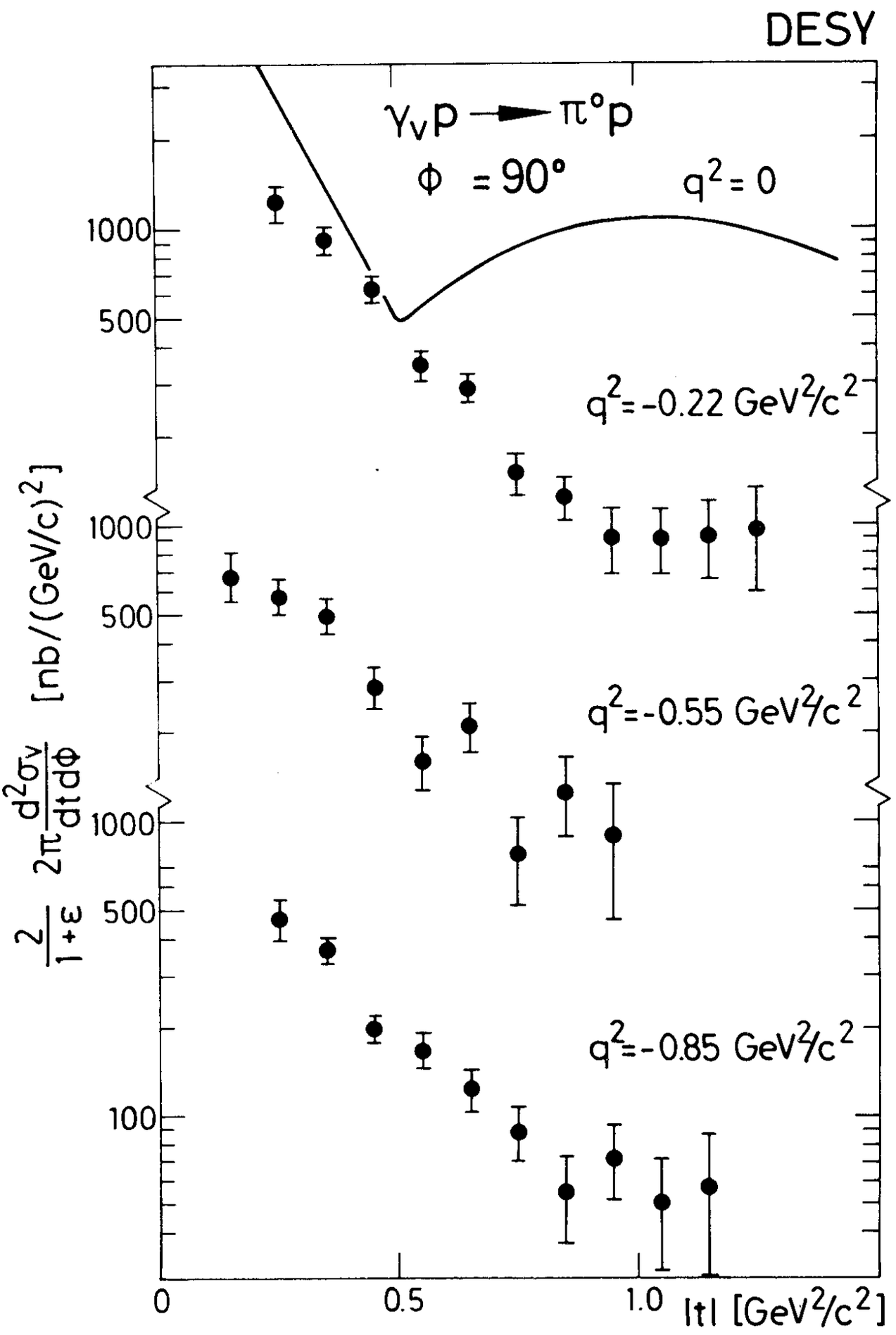
DESY
$\gamma_v p \rightarrow \pi^0 p$
$\phi = 90°$
$q^2 = 0$
$q^2 = -0.22\ GeV^2/c^2$
$q^2 = -0.55\ GeV^2/c^2$
$q^2 = -0.85\ GeV^2/c^2$
$\frac{2}{1+\varepsilon} 2\pi \frac{d^2\sigma_v}{dt d\phi}$ [nb/(GeV/c)$^2$]
1000
500
1000
500
1000
500
100
0
0.5
1.0
|t| [GeV$^2$/c$^2$]

Fig. 6

23970

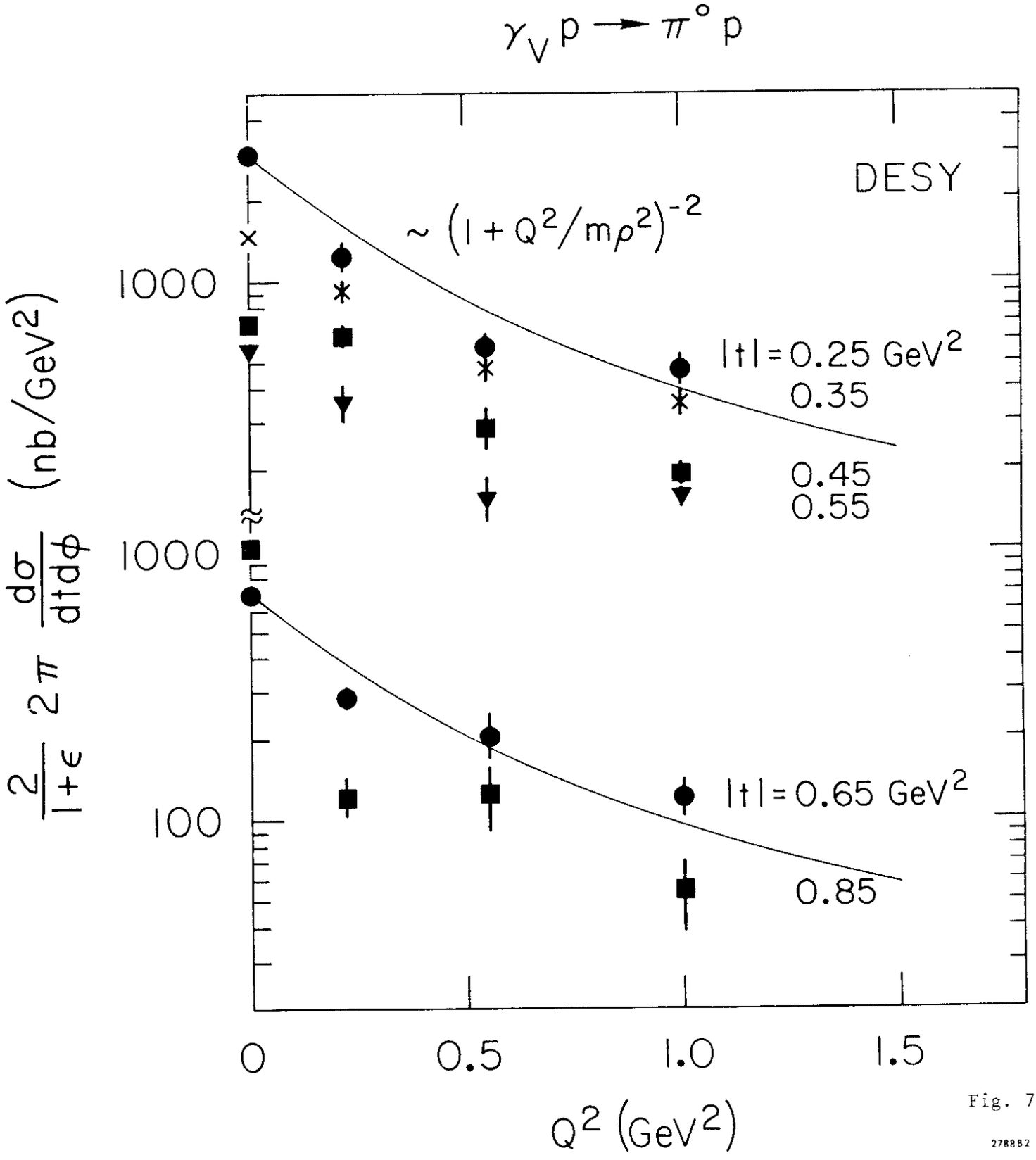
$\gamma_V p \rightarrow \pi^\circ p$
DESY
$\sim (1 + Q^2/m\rho^2)^{-2}$
$|t| = 0.25$ GeV$^2$
0.35
0.45
0.55
$|t| = 0.65$ GeV$^2$
0.85
1000
1000
100
$\frac{2}{1+\epsilon} 2\pi \frac{d\sigma}{dt d\phi}$ (nb/GeV$^2$)
0
0.5
1.0
1.5
$Q^2$ (GeV$^2$)

Fig. 7

278882

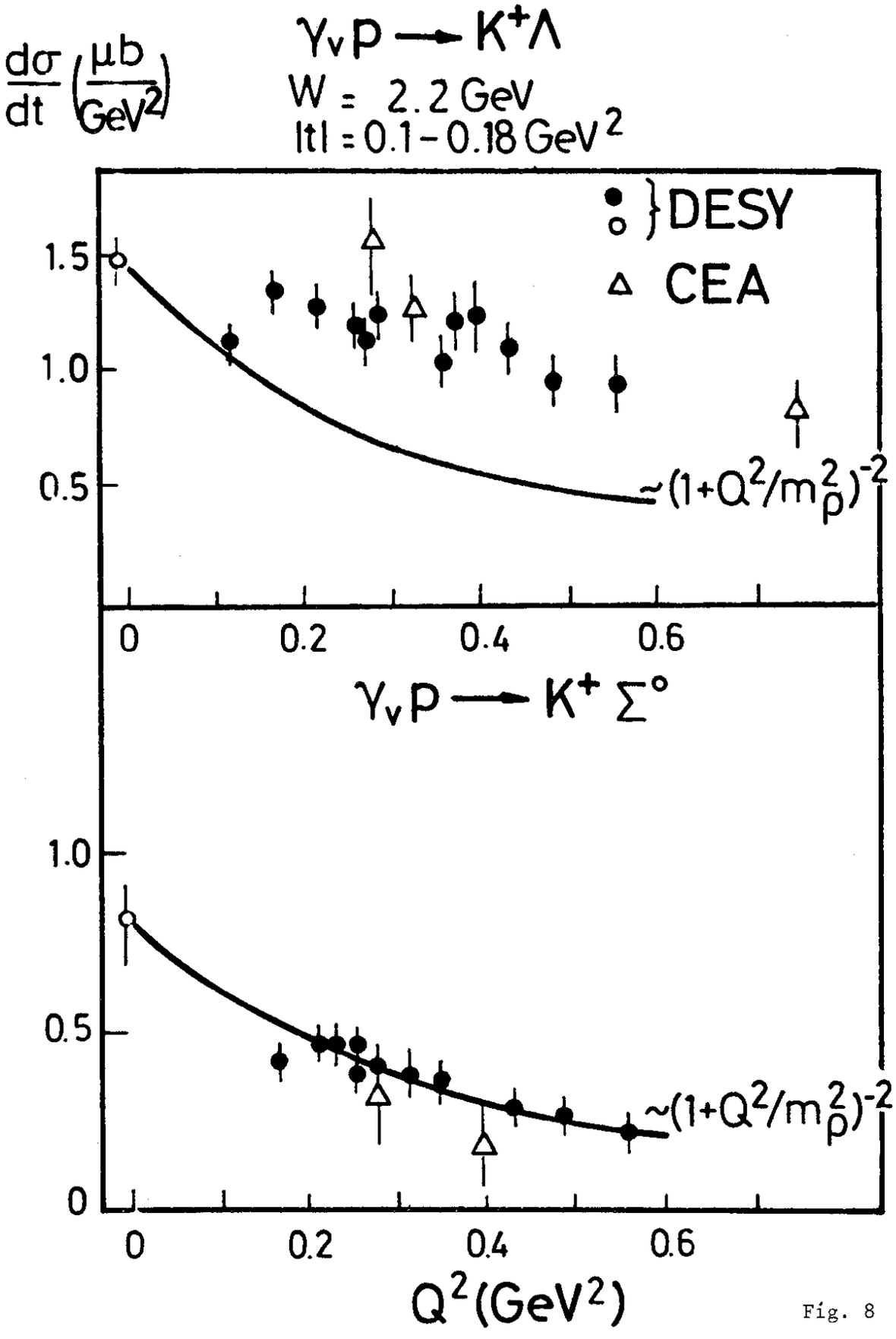
$\frac{d\sigma}{dt}\left(\frac{\mu b}{GeV^2}\right)$
$\gamma_v P \rightarrow K^+\Lambda$
W = 2.2 GeV
$|t| = 0.1 - 0.18\ GeV^2$
DESY
CEA
$\sim(1+Q^2/m_\rho^2)^{-2}$
1.5
1.0
0.5
0
0.2
0.4
0.6
$\gamma_v P \rightarrow K^+\Sigma^\circ$
1.0
0.5
0
$\sim(1+Q^2/m_\rho^2)^{-2}$
0
0.2
0.4
0.6
$Q^2(GeV^2)$

Fig. 8

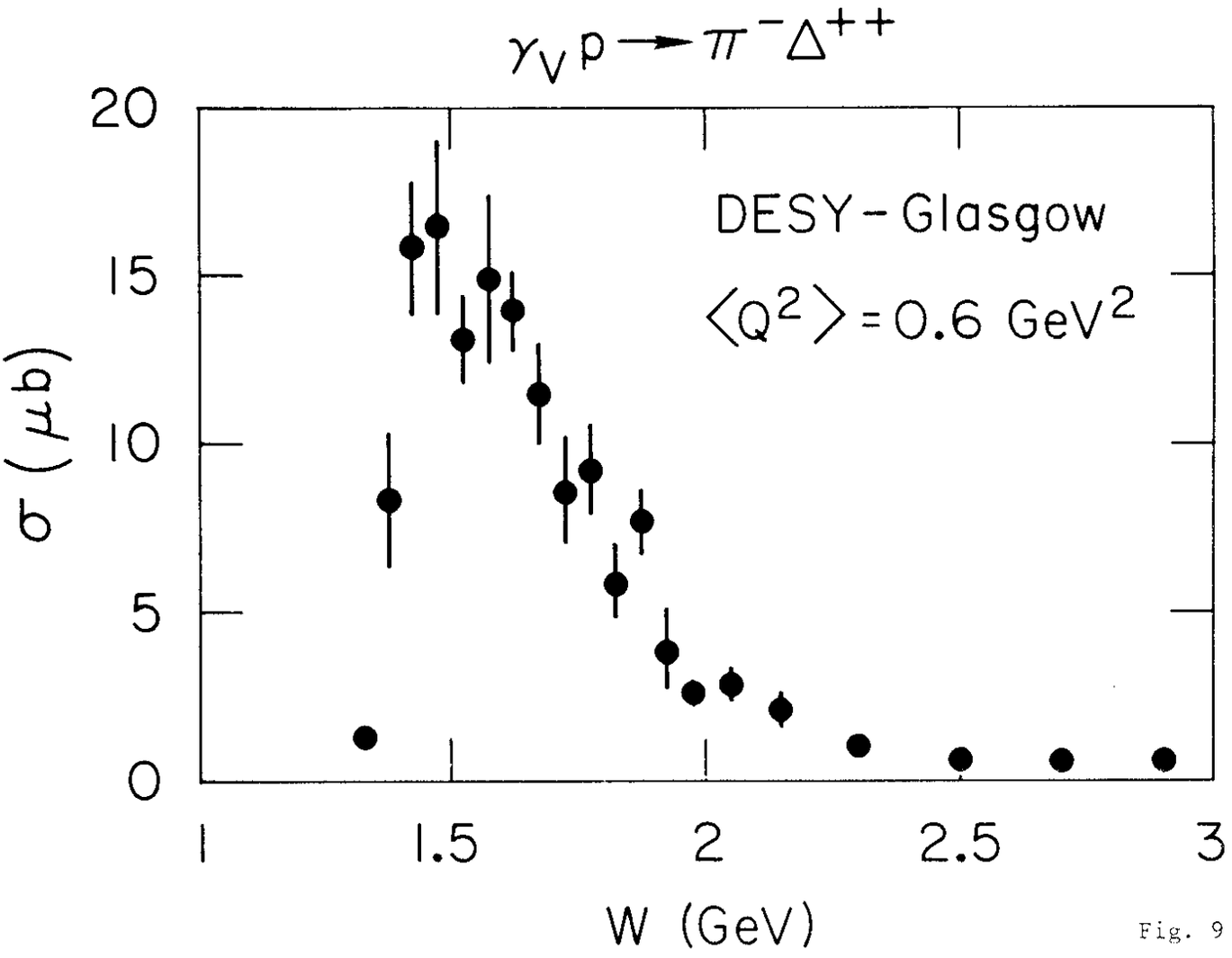
$\gamma_V p \rightarrow \pi^- \Delta^{++}$
DESY - Glasgow
$\langle Q^2 \rangle = 0.6$ GeV$^2$
$\sigma$ ($\mu$b)
W (GeV)
0
5
10
15
20
1
1.5
2
2.5
3

Fig. 9

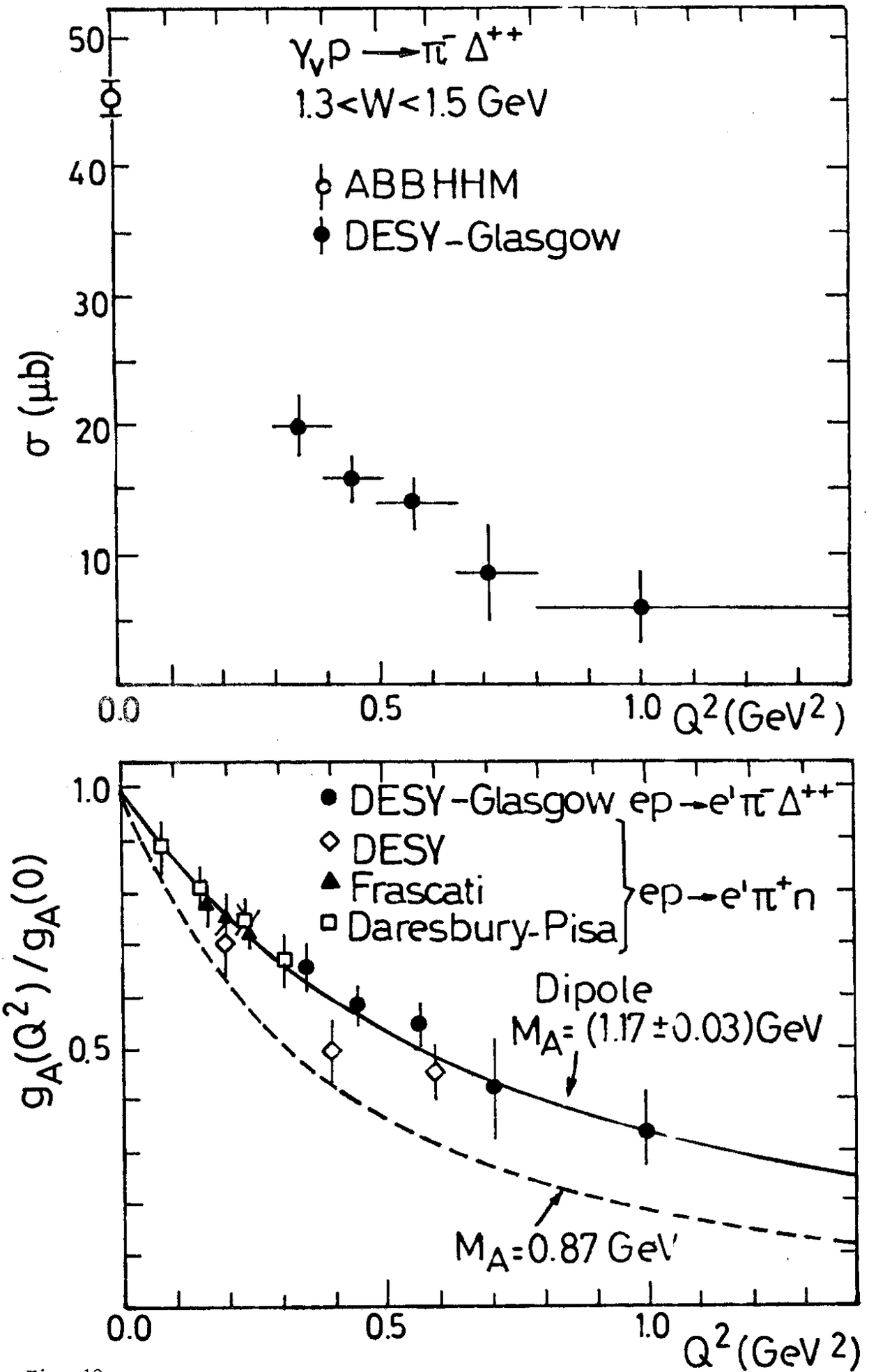
$\gamma_v p \rightarrow \pi^- \Delta^{++}$
1.3<W<1.5 GeV
ABBHHM
DESY-Glasgow
σ (μb)
50
40
30
20
10
0.0
0.5
1.0
$Q^2$ (GeV$^2$)
DESY-Glasgow $ep \rightarrow e'\pi^-\Delta^{++}$
DESY
Frascati
Daresbury-Pisa
$ep \rightarrow e'\pi^+ n$
Dipole
$M_A = (1.17 \pm 0.03)$ GeV
$M_A = 0.87$ GeV
$g_A(Q^2)/g_A(0)$
1.0
0.5
0.0
0.5
1.0
$Q^2$ (GeV$^2$)

Fig. 10

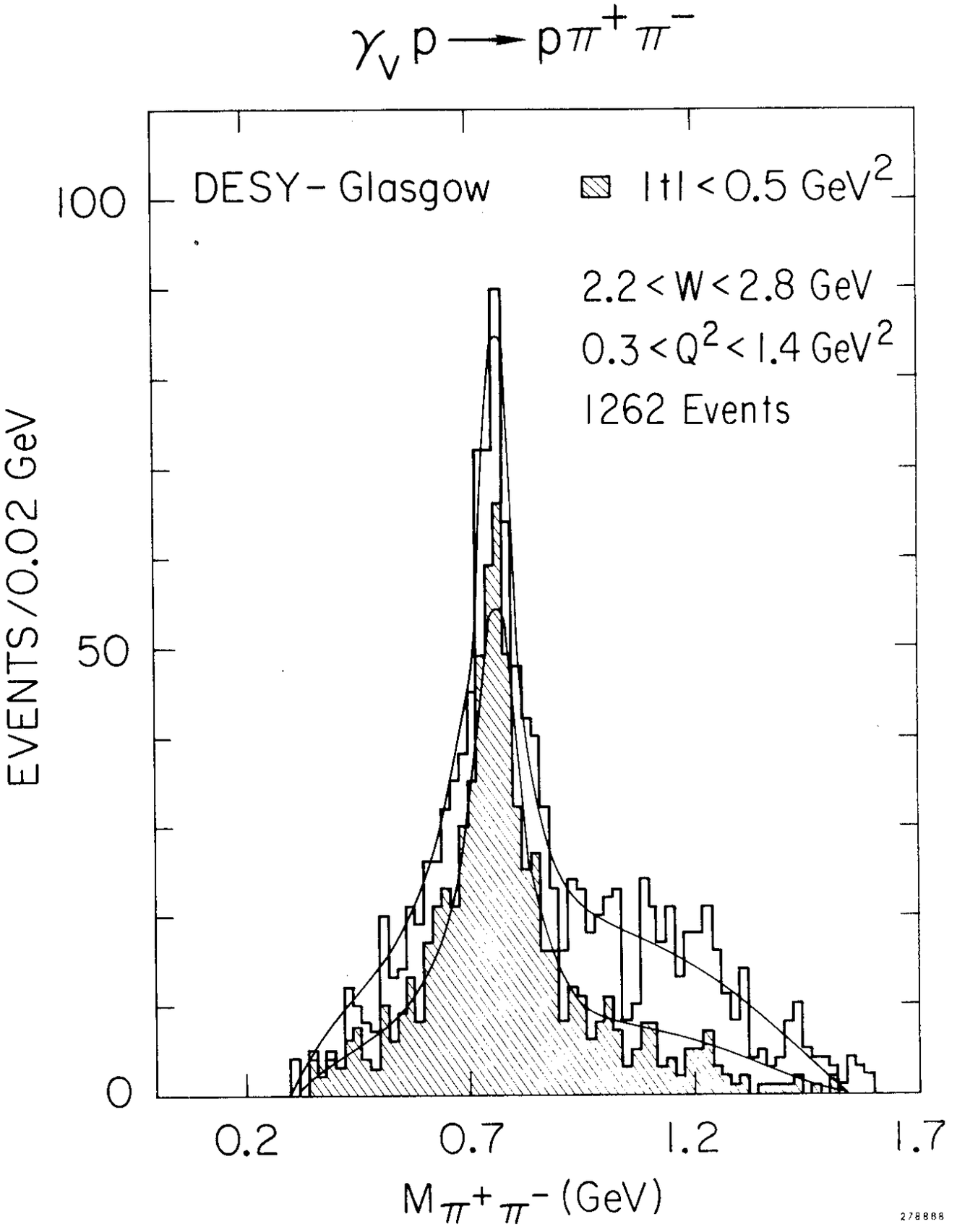
$\gamma_V p \longrightarrow p\pi^+\pi^-$
DESY - Glasgow
$|t| < 0.5$ GeV$^2$
$2.2 < W < 2.8$ GeV
$0.3 < Q^2 < 1.4$ GeV$^2$
1262 Events
EVENTS/0.02 GeV
100
50
0
0.2
0.7
1.2
1.7
$M_{\pi^+\pi^-}$ (GeV)
278888

Fig. 11

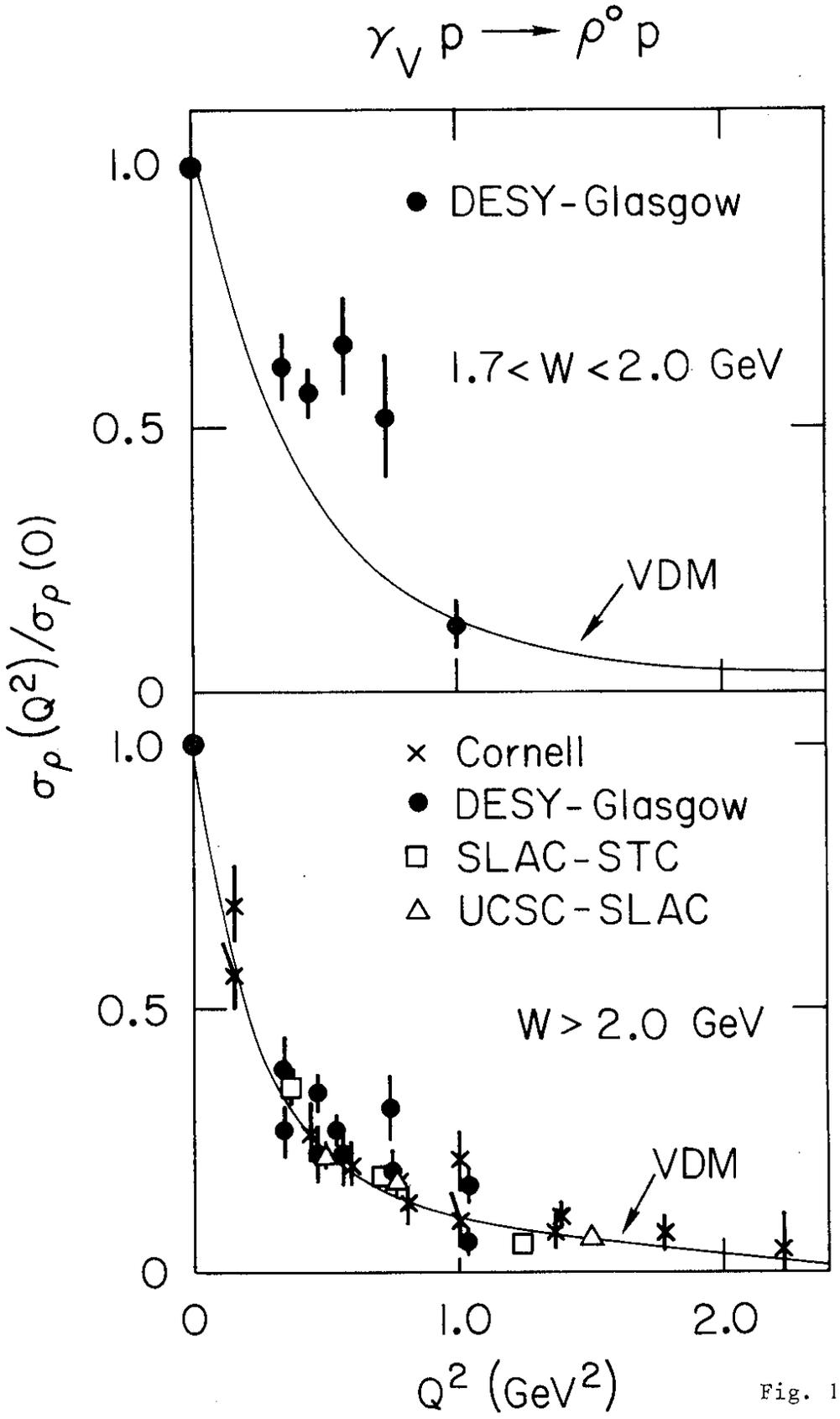
$\gamma_V p \longrightarrow \rho^\circ p$
1.0
0.5
0
DESY-Glasgow
1.7< W <2.0 GeV
VDM
1.0
0.5
0
Cornell
DESY-Glasgow
SLAC-STC
UCSC-SLAC
W > 2.0 GeV
VDM
$\sigma_\rho(Q^2)/\sigma_\rho(0)$
0
1.0
2.0
$Q^2$ (GeV$^2$)

Fig. 12

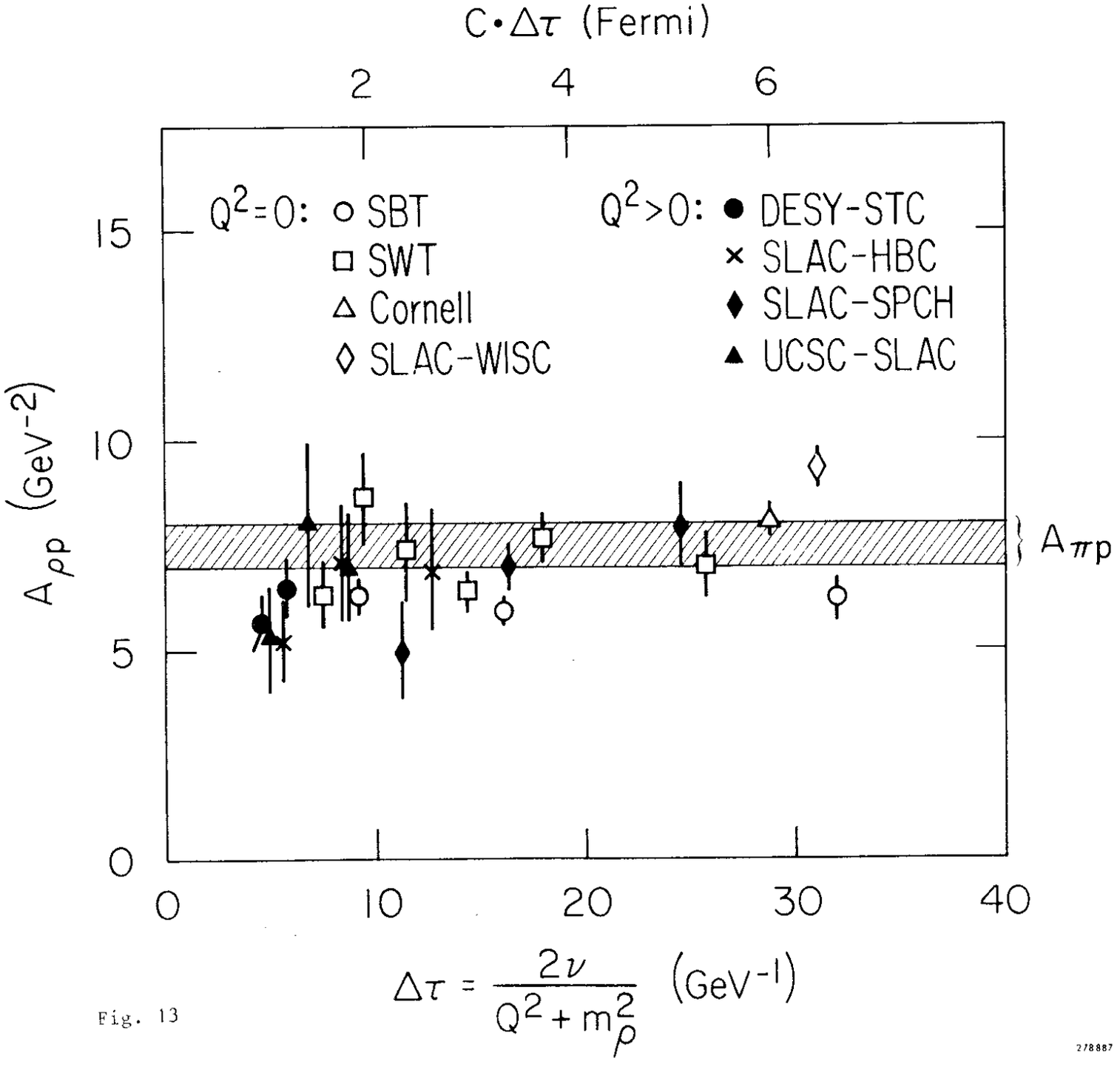
C·Δτ (Fermi)
2
4
6
$Q^2=0$: ○ SBT
□ SWT
△ Cornell
◇ SLAC-WISC
$Q^2>0$: ● DESY-STC
× SLAC-HBC
♦ SLAC-SPCH
▲ UCSC-SLAC
15
10
5
0
$A_{\rho p}$ (GeV$^{-2}$)
$A_{\pi p}$
0
10
20
30
40
$\Delta\tau = \frac{2\nu}{Q^2 + m_\rho^2}$ (GeV$^{-1}$)

Fig. 13

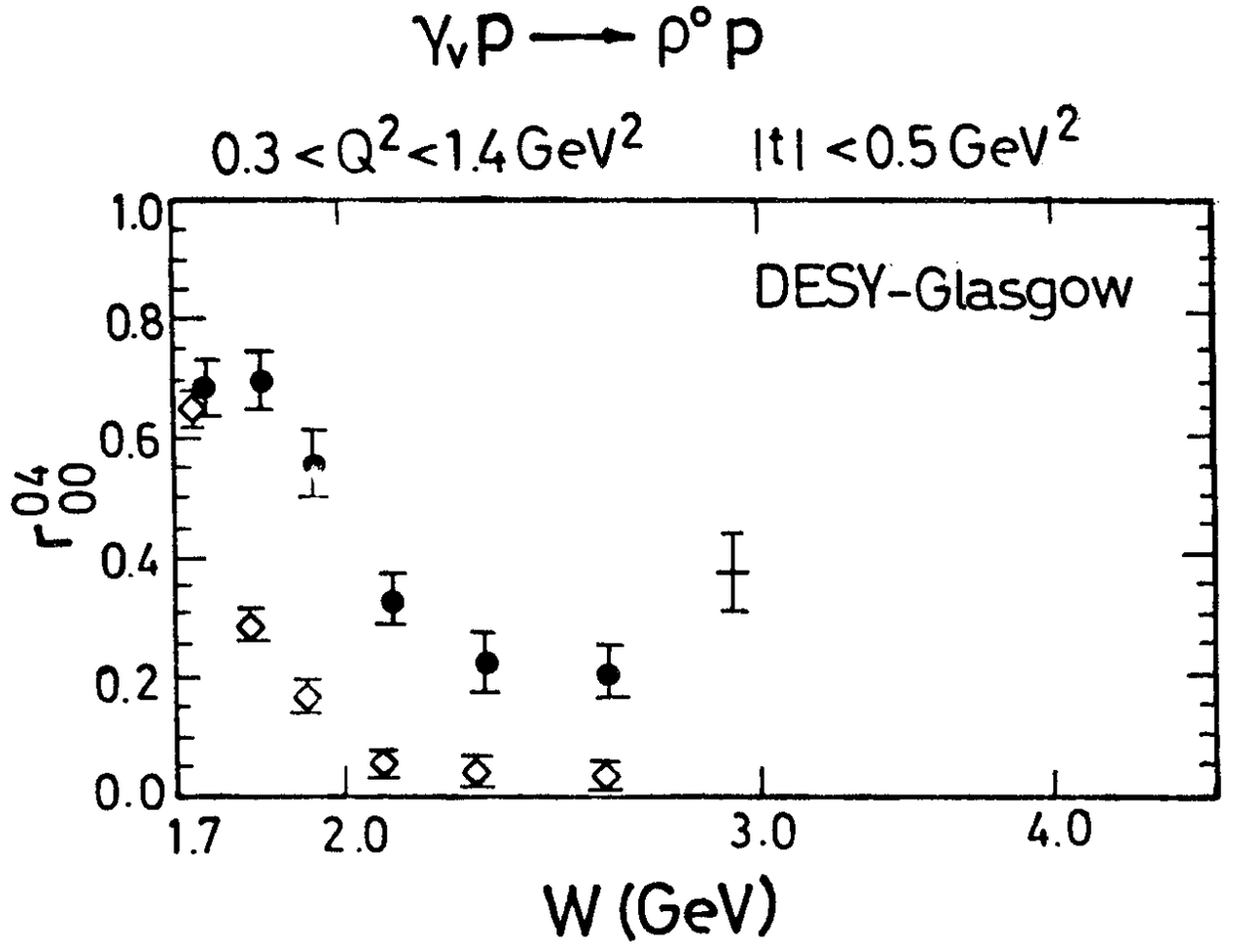
$\gamma_v p \longrightarrow \rho^0 p$
$0.3 < Q^2 < 1.4\,GeV^2$
$|t| < 0.5\,GeV^2$
DESY-Glasgow
$r^{04}_{00}$
1.0
0.8
0.6
0.4
0.2
0.0
1.7
2.0
3.0
4.0
W (GeV)

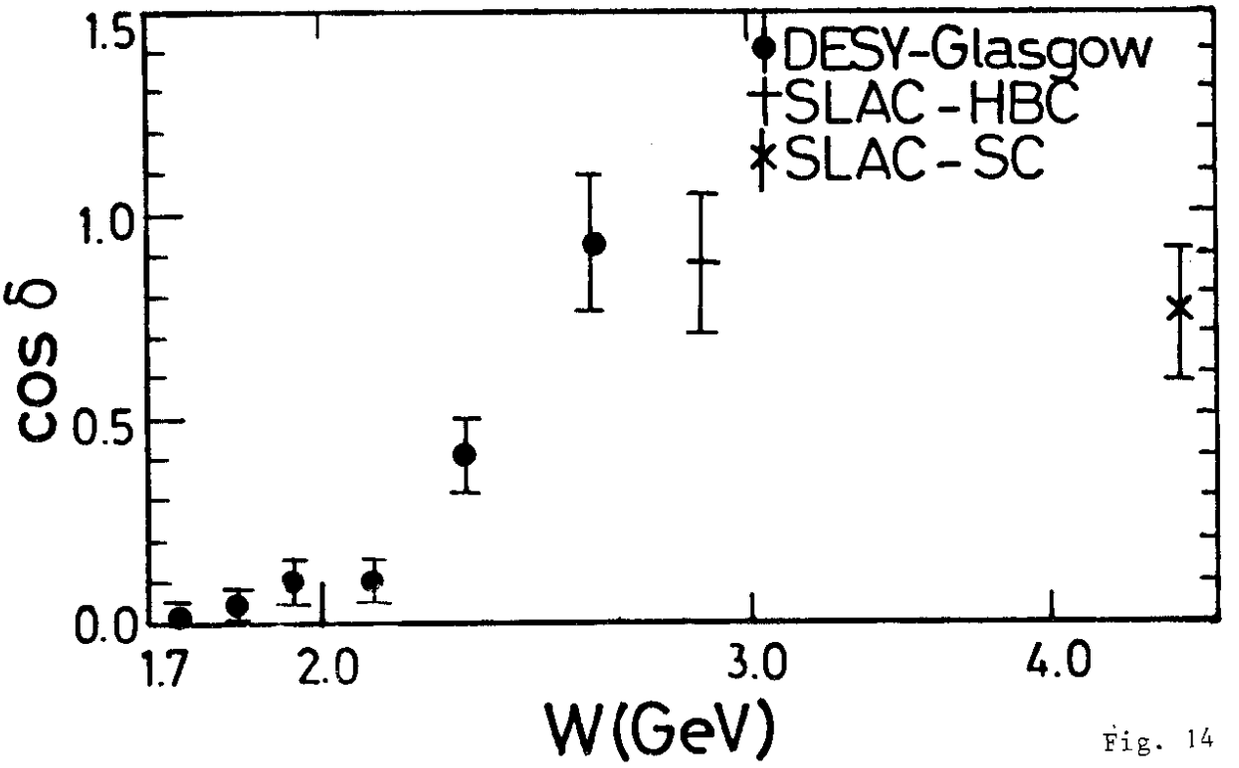
DESY-Glasgow
SLAC-HBC
SLAC-SC
cos δ
1.5
1.0
0.5
0.0
1.7
2.0
3.0
4.0
W(GeV)

Fig. 14

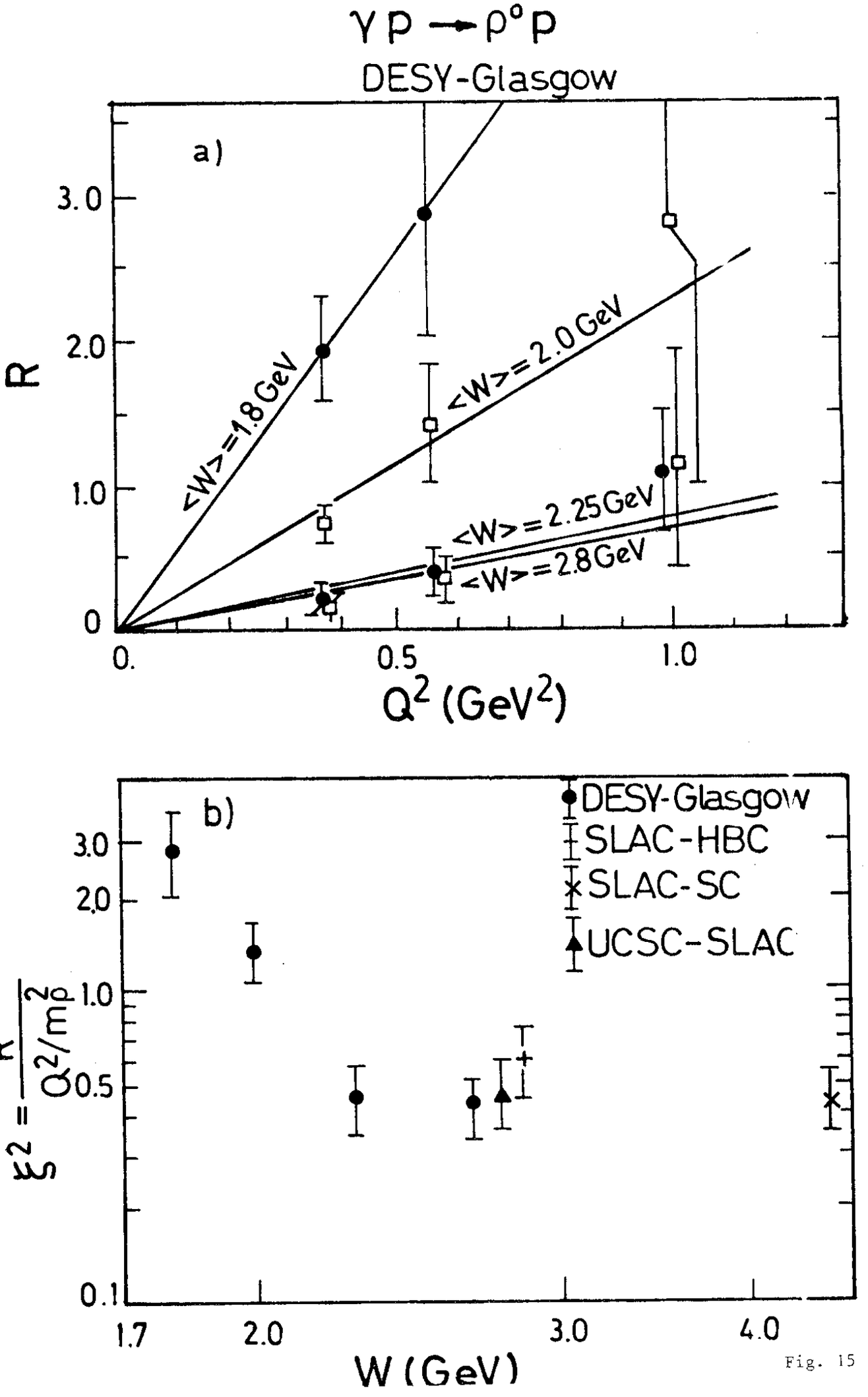
γ p → ρ° p
DESY-Glasgow
a)
R
3.0
2.0
1.0
0
0.
0.5
1.0
Q² (GeV²)
<W>=1.8GeV
<W>=2.0GeV
<W>=2.25GeV
<W>=2.8GeV
b)
DESY-Glasgow
SLAC-HBC
SLAC-SC
UCSC-SLAC
ξ² = R / (Q²/m²ρ)
3.0
2.0
1.0
0.5
0.1
1.7
2.0
3.0
4.0
W (GeV)

Fig. 15

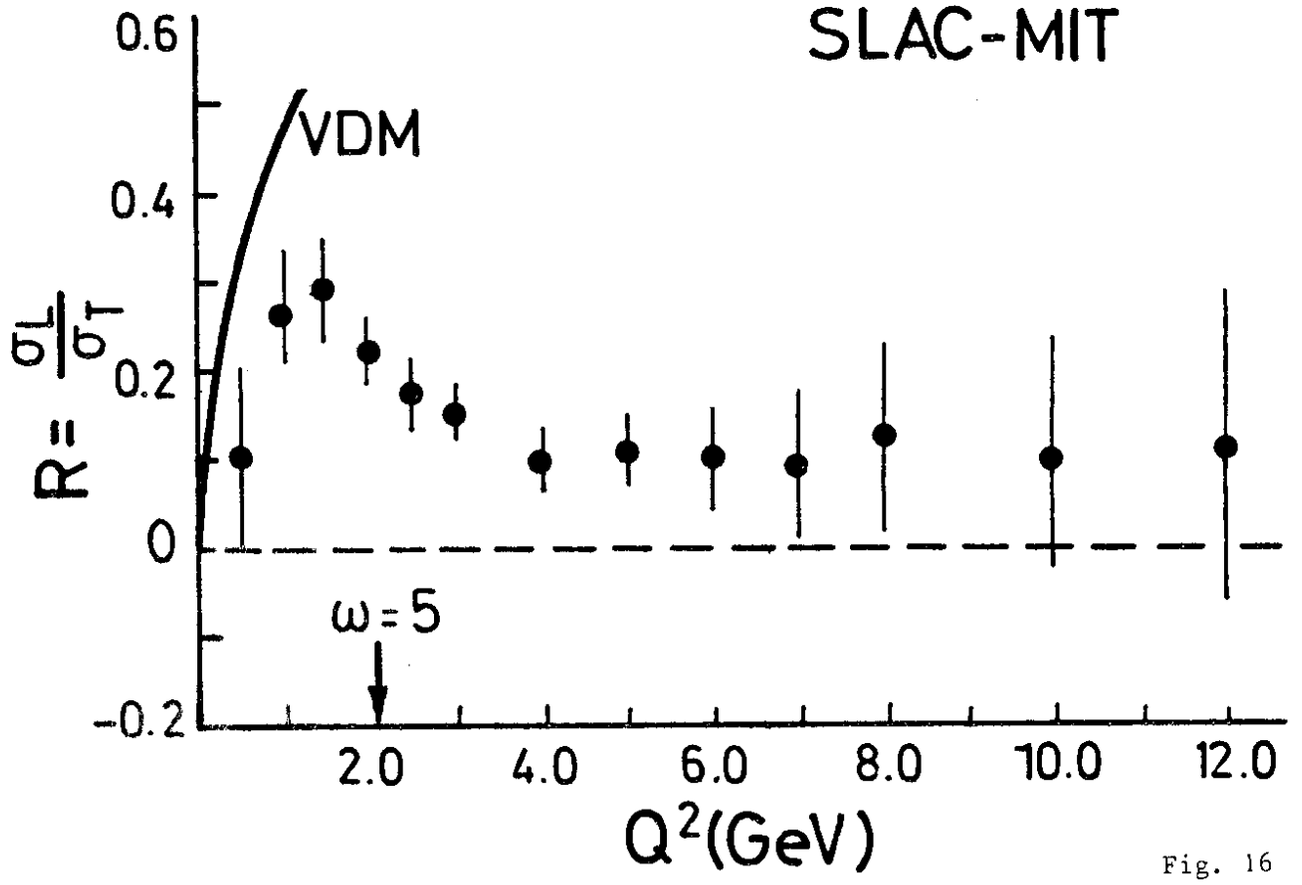
SLAC-MIT
VDM
0.6
0.4
0.2
0
-0.2
$R = \frac{\sigma_L}{\sigma_T}$
ω = 5
2.0
4.0
6.0
8.0
10.0
12.0
$Q^2$(GeV)

Fig. 16

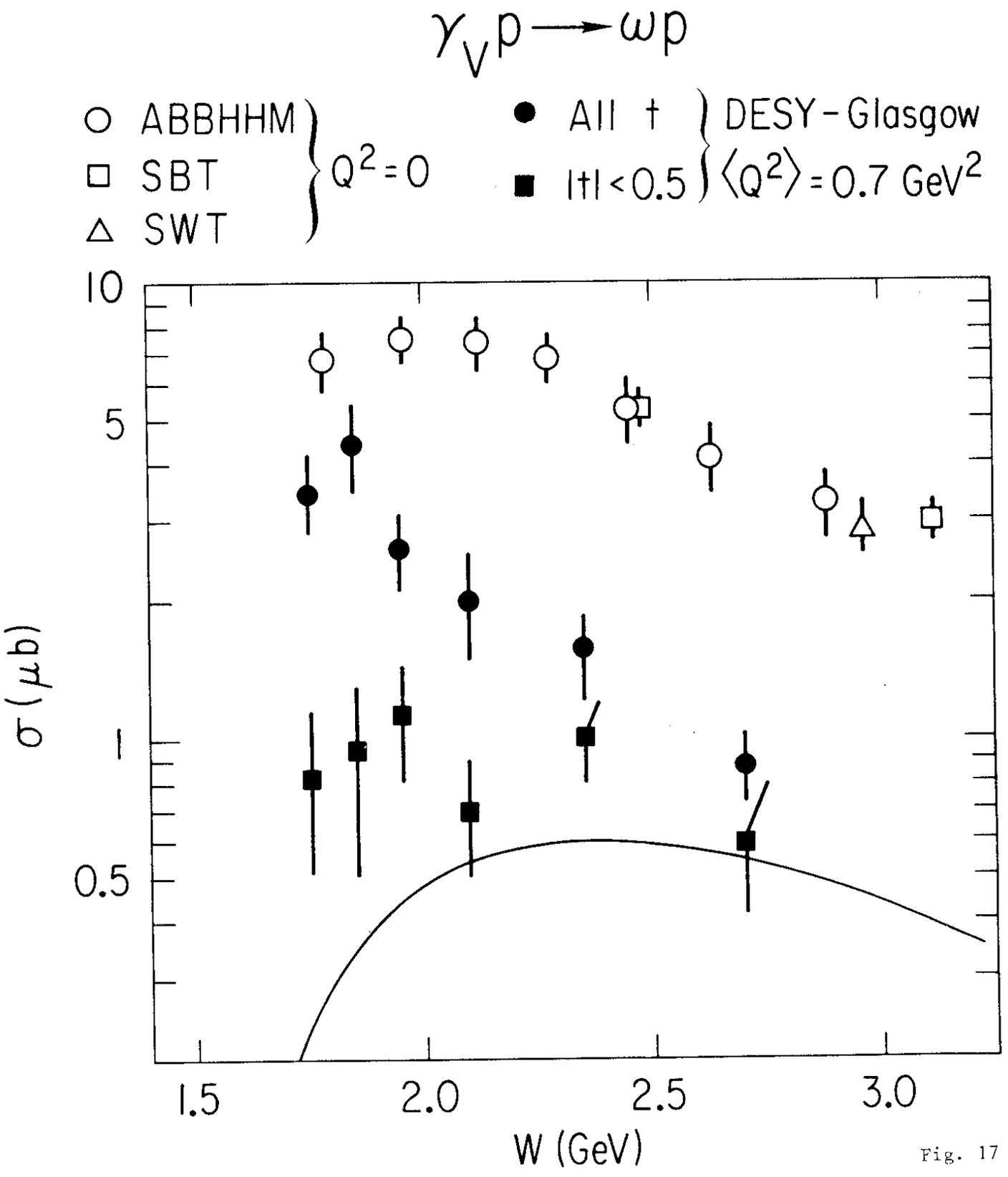
$\gamma_V p \rightarrow \omega p$
ABBHHM
SBT
SWT
$Q^2 = 0$
All t
$|t| < 0.5$
DESY - Glasgow
$\langle Q^2 \rangle = 0.7$ GeV$^2$
10
5
1
0.5
$\sigma$ ($\mu$b)
1.5
2.0
2.5
3.0
W (GeV)

Fig. 17

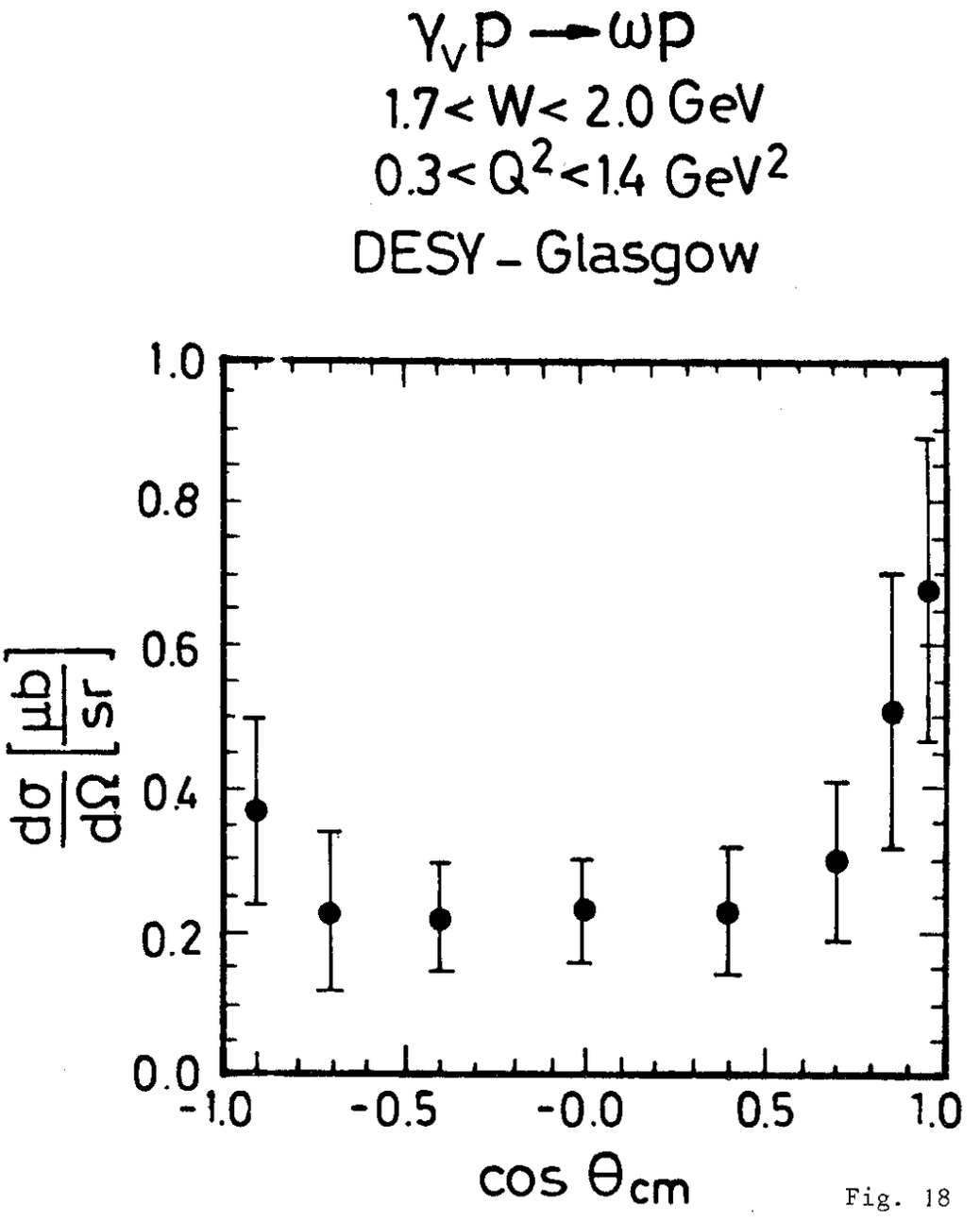
$\gamma_v p \rightarrow \omega p$
$1.7 < W < 2.0$ GeV
$0.3 < Q^2 < 1.4$ GeV$^2$
DESY – Glasgow
$\frac{d\sigma}{d\Omega}\left[\frac{\mu b}{sr}\right]$
1.0
0.8
0.6
0.4
0.2
0.0
-1.0
-0.5
-0.0
0.5
1.0
$\cos\Theta_{cm}$

Fig. 18

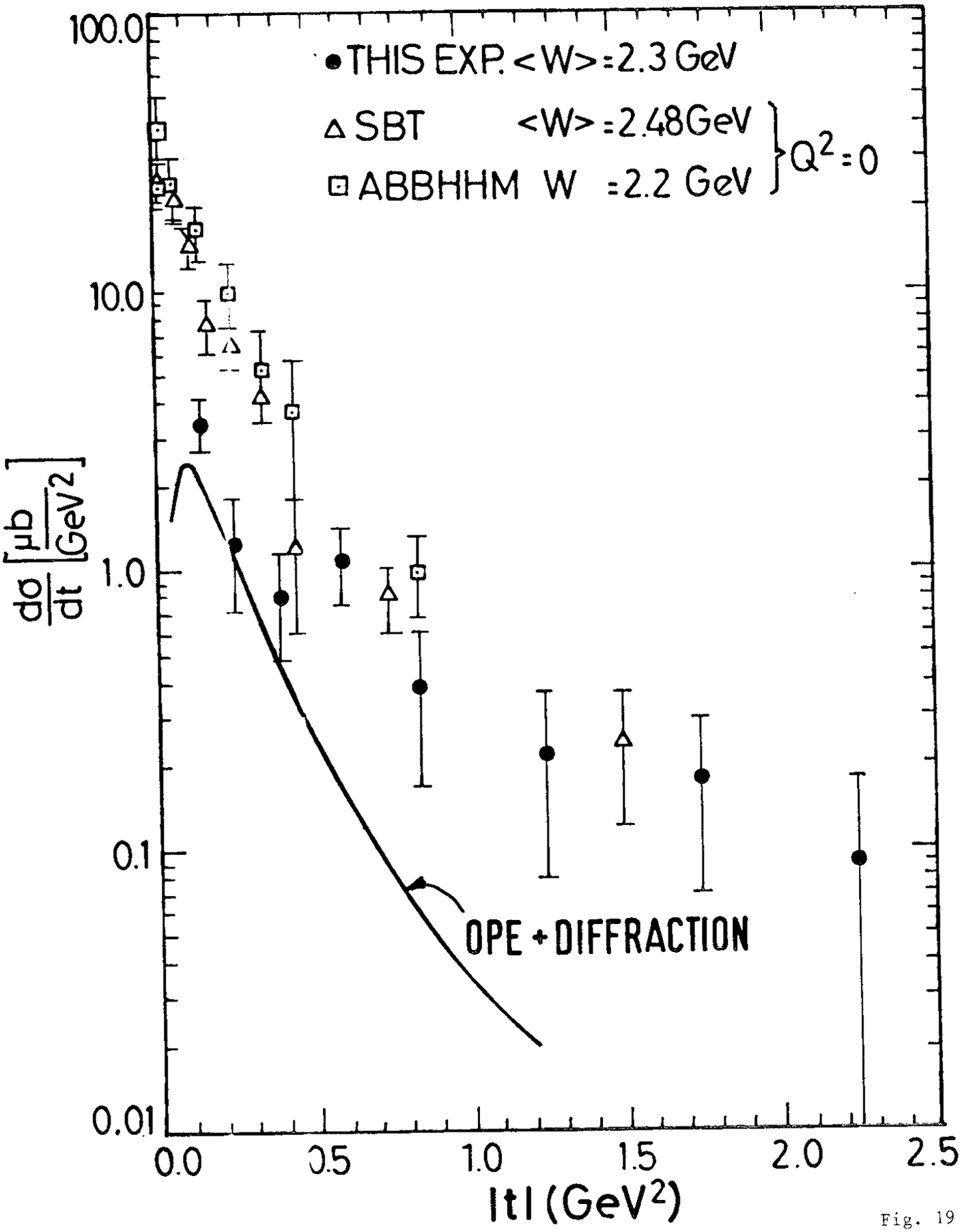
$\gamma_v P \longrightarrow \omega P$
$2.0 < W < 2.8$ GeV
$0.3 < Q^2 < 1.4$ GeV$^2$ DESY-Glasgow
THIS EXP. <W> = 2.3 GeV
SBT <W> = 2.48 GeV
ABBHHM W = 2.2 GeV
$Q^2 = 0$
OPE + DIFFRACTION
$\frac{d\sigma}{dt}$ [$\frac{\mu b}{GeV^2}$]
100.0
10.0
1.0
0.1
0.01
0.0
0.5
1.0
1.5
2.0
2.5
$|t|$ (GeV$^2$)

Fig. 19

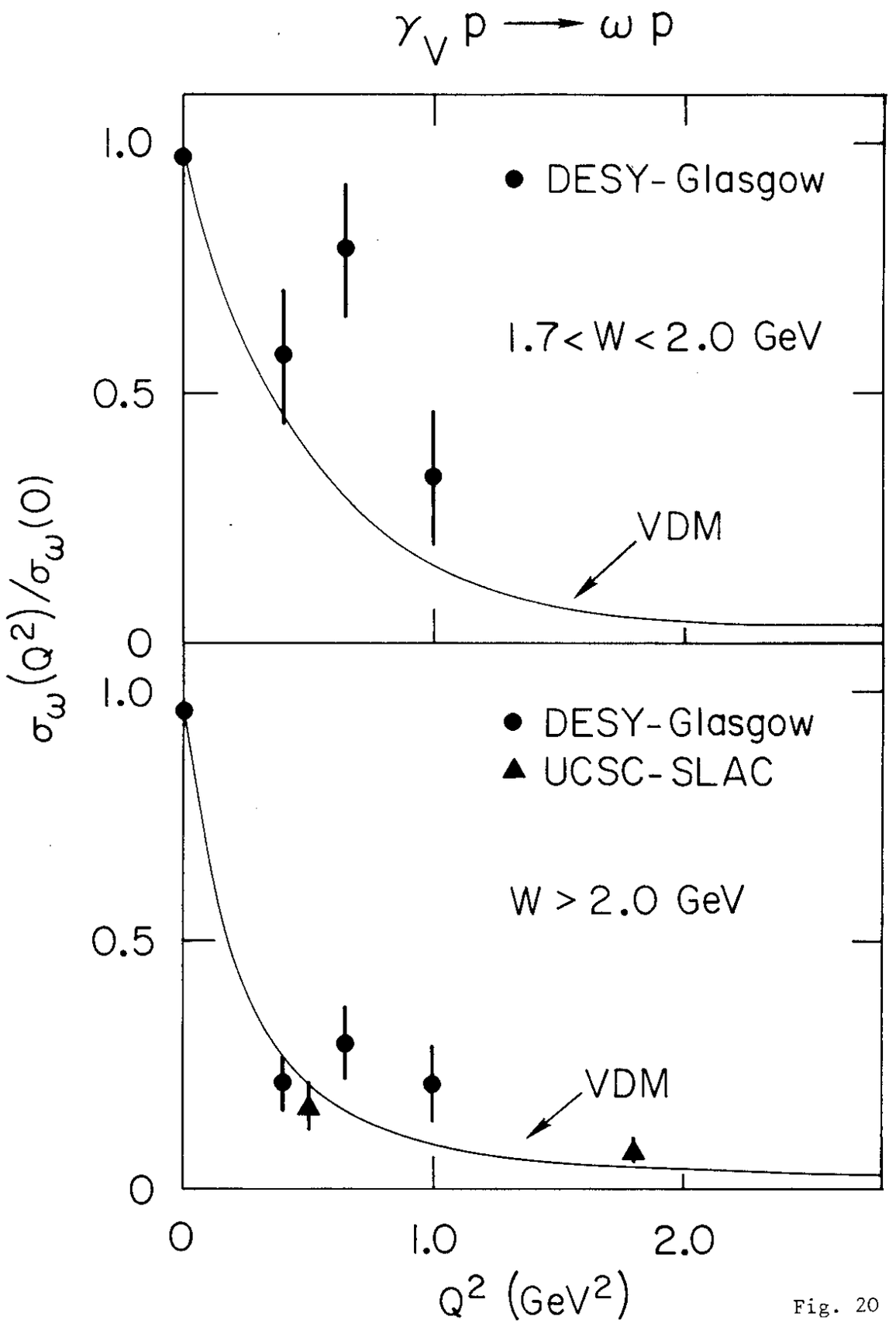
$\gamma_V p \longrightarrow \omega p$
1.0
0.5
0
DESY-Glasgow
1.7<W<2.0 GeV
VDM
1.0
0.5
0
DESY-Glasgow
UCSC-SLAC
W > 2.0 GeV
VDM
$\sigma_\omega(Q^2)/\sigma_\omega(0)$
0
1.0
2.0
$Q^2$ (GeV$^2$)

Fig. 20

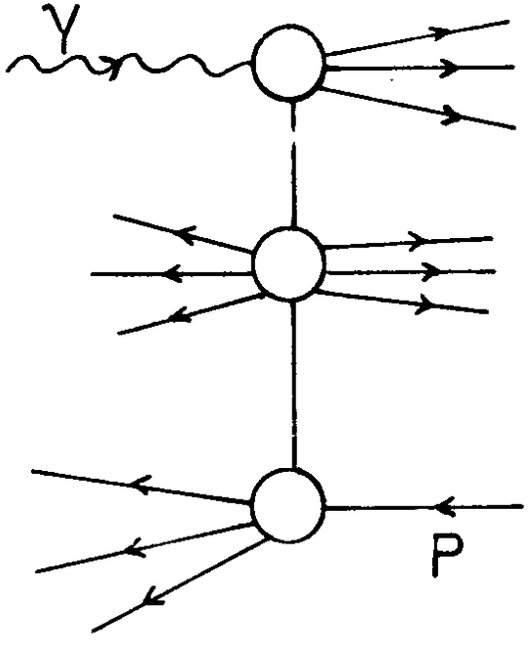


$x > 0$ beam fragmentation

$x \approx 0$ central region

$x < 0$ target fragmentation

Fig 21

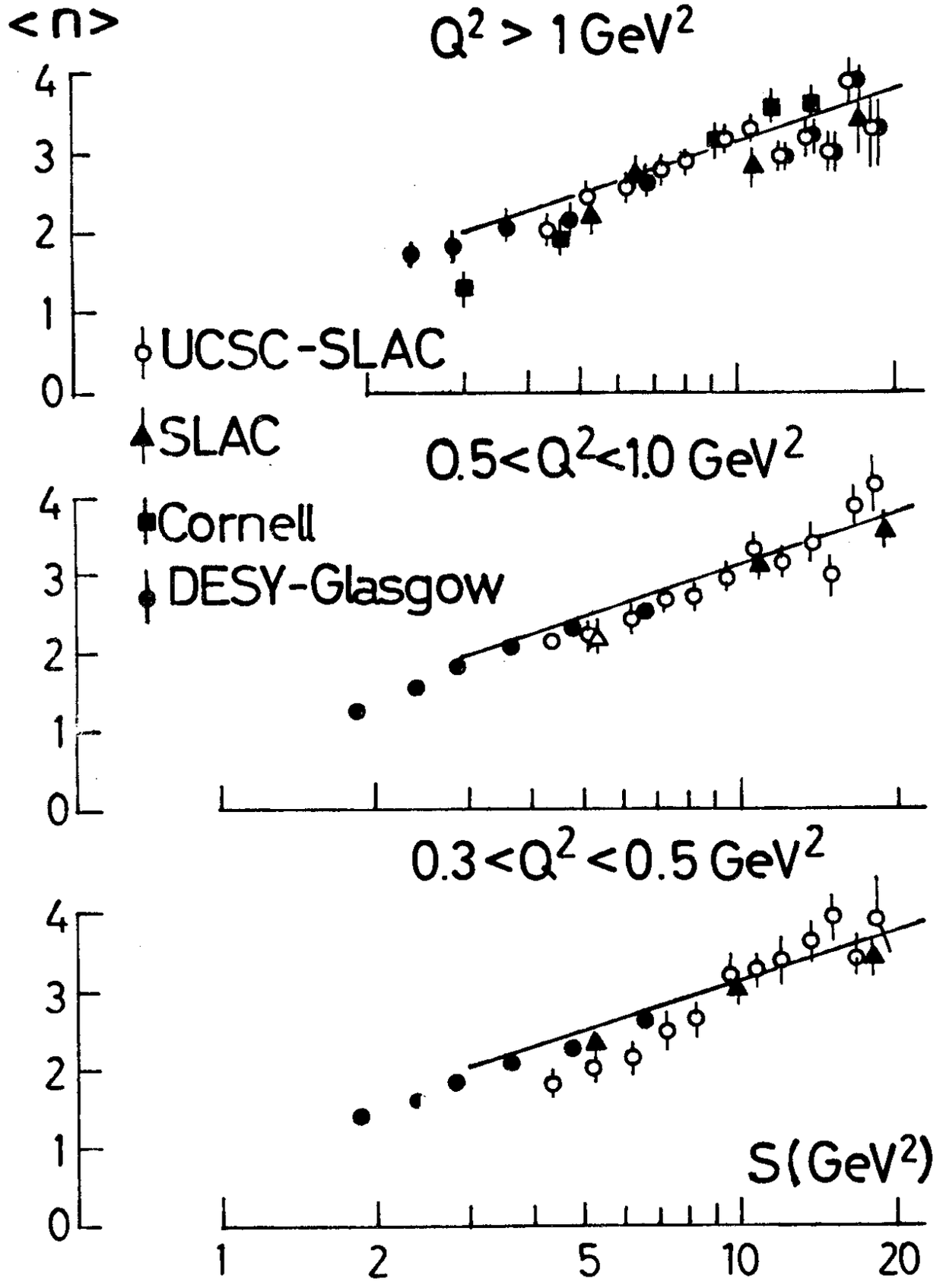
<n>
$Q^2 > 1\,GeV^2$
UCSC-SLAC
SLAC
$0.5 < Q^2 < 1.0\,GeV^2$
Cornell
DESY-Glasgow
$0.3 < Q^2 < 0.5\,GeV^2$
S(GeV²)
0
1
2
3
4
1
2
5
10
20

Fig. 22

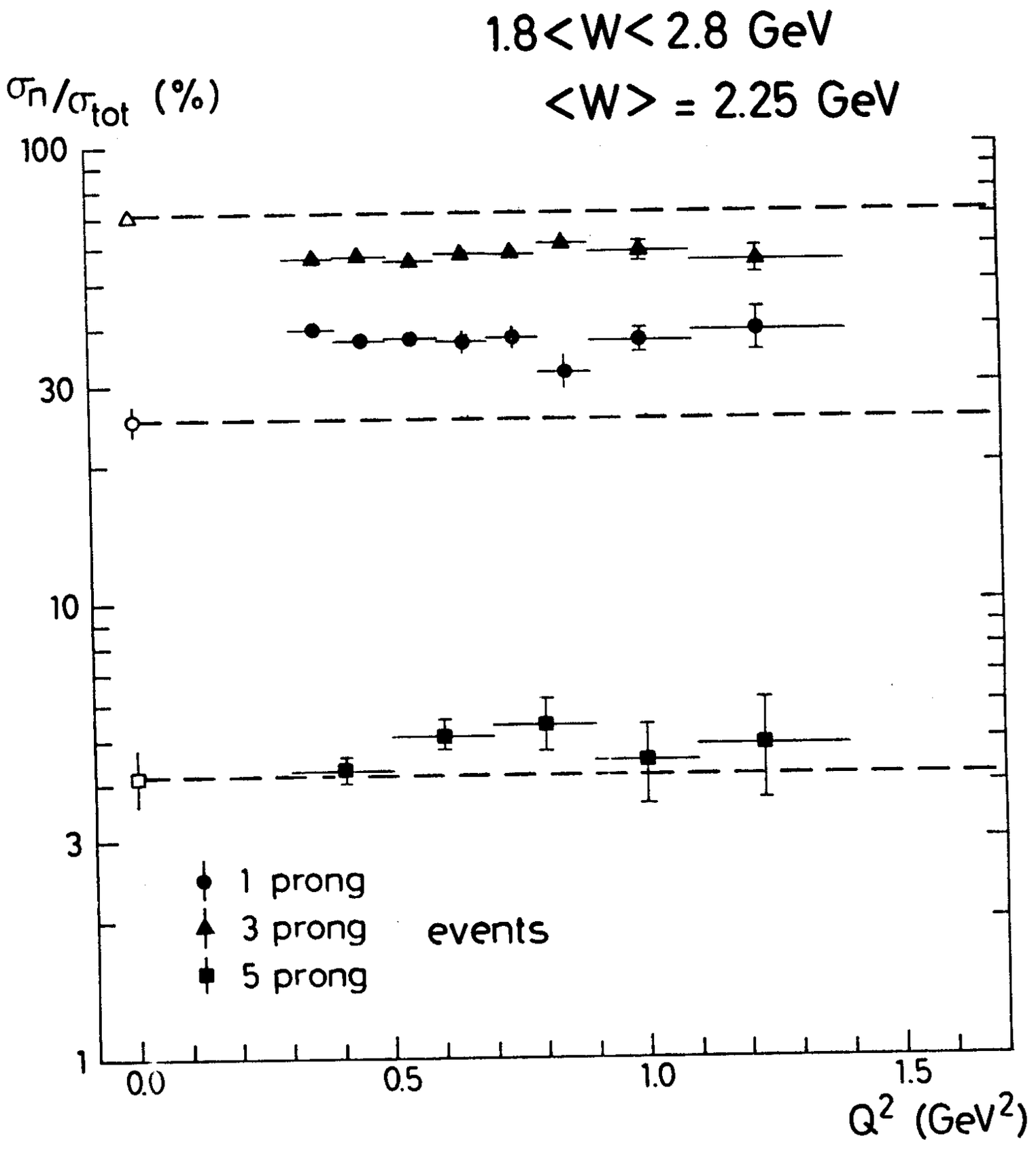
1.8<W<2.8 GeV
<W> = 2.25 GeV
σn/σtot (%)
100
30
10
3
1
1 prong
3 prong
5 prong
events
0.0
0.5
1.0
1.5
Q² (GeV²)

Fig. 23

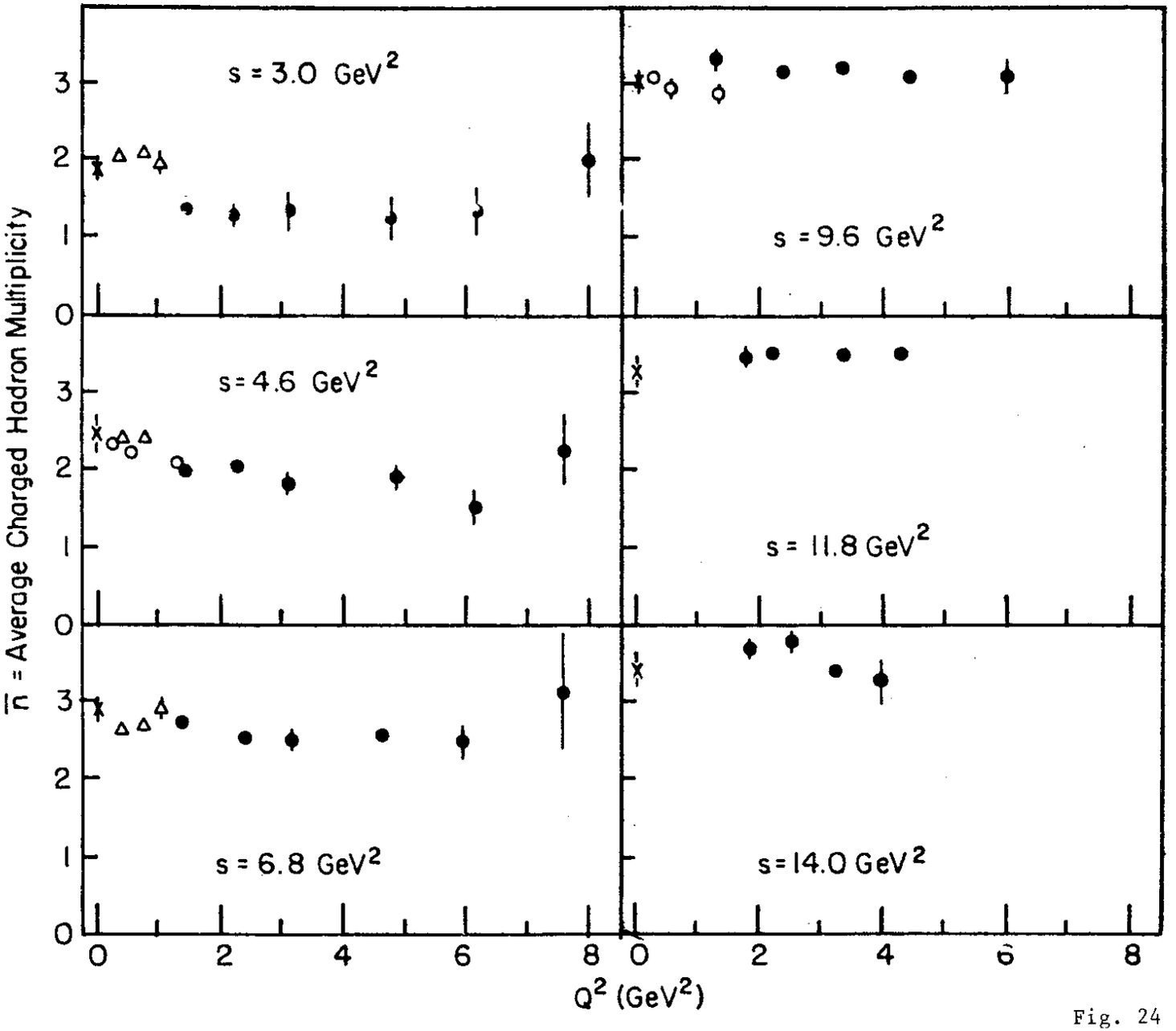
s = 3.0 GeV²
s = 9.6 GeV²
s = 4.6 GeV²
s = 11.8 GeV²
s = 6.8 GeV²
s = 14.0 GeV²
n̄ = Average Charged Hadron Multiplicity
Q² (GeV²)
0
1
2
3
4
6
8

Fig. 24

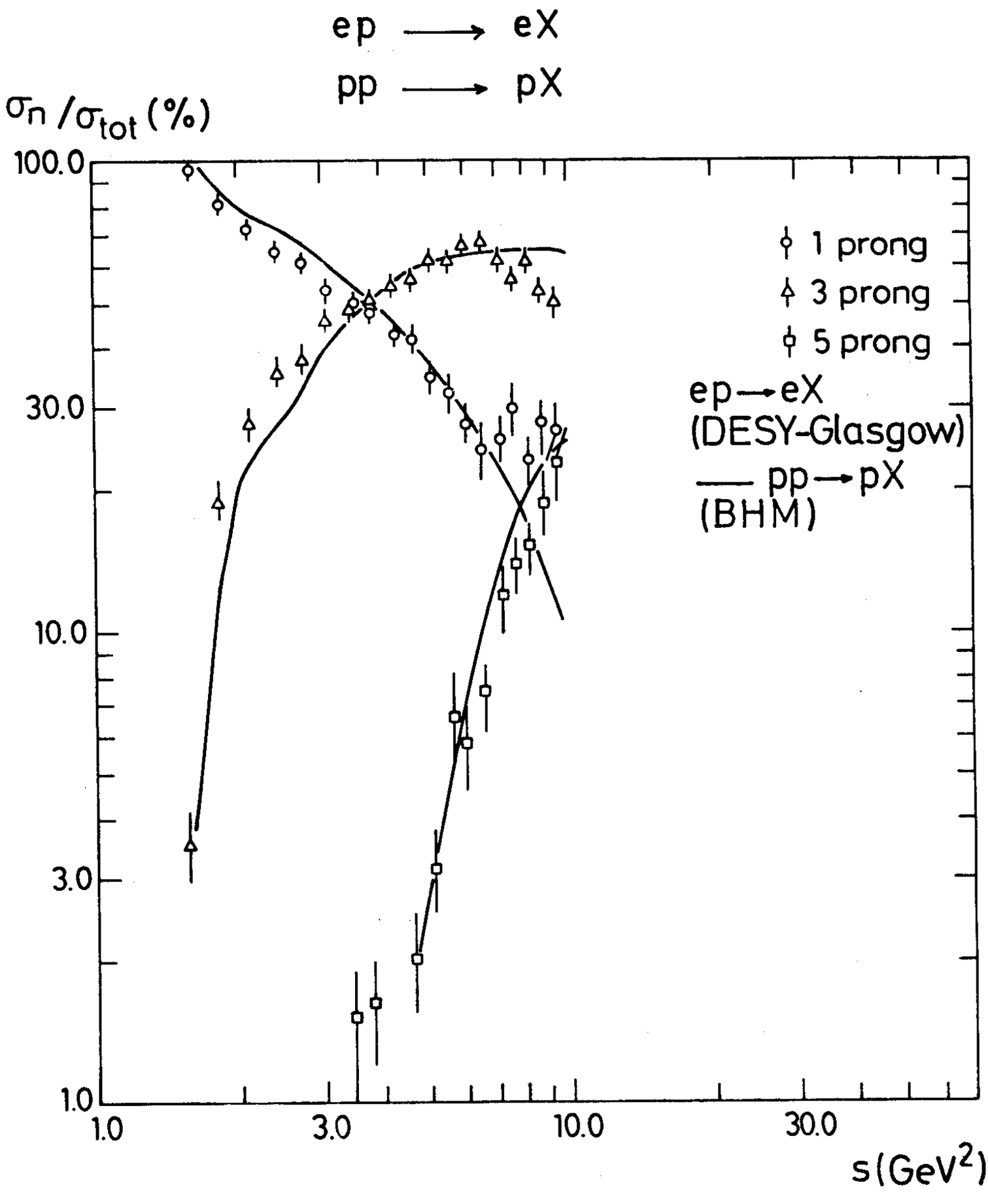
ep ⟶ eX
pp ⟶ pX
σn /σtot (%)
100.0
30.0
10.0
3.0
1.0
1.0
3.0
10.0
30.0
s(GeV²)
1 prong
3 prong
5 prong
ep→eX
(DESY-Glasgow)
pp→pX
(BHM)

Fig. 25

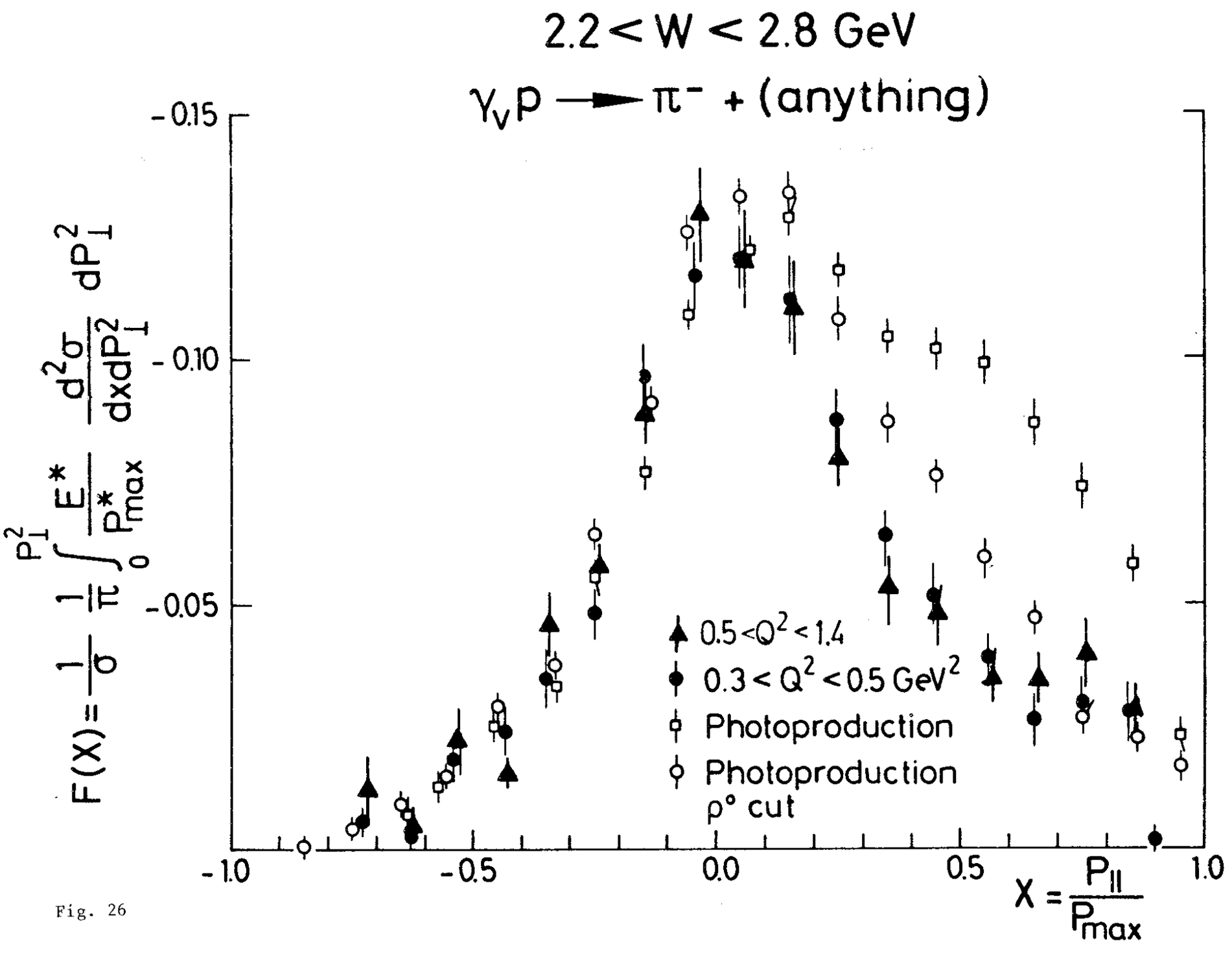
2.2 < W < 2.8 GeV
$\gamma_v p \longrightarrow \pi^- + (\text{anything})$
$F(X) = \frac{1}{\sigma} \frac{1}{\pi} \int_0^{P_\perp^2} \frac{E^*}{P^*_{max}} \frac{d^2\sigma}{dx dP_\perp^2} dP_\perp^2$
- 0.15
- 0.10
- 0.05
-1.0
-0.5
0.0
0.5
1.0
$X = \frac{P_{||}}{P_{max}}$
$0.5 < Q^2 < 1.4$
$0.3 < Q^2 < 0.5\ GeV^2$
Photoproduction
Photoproduction
ρ° cut

Fig. 26

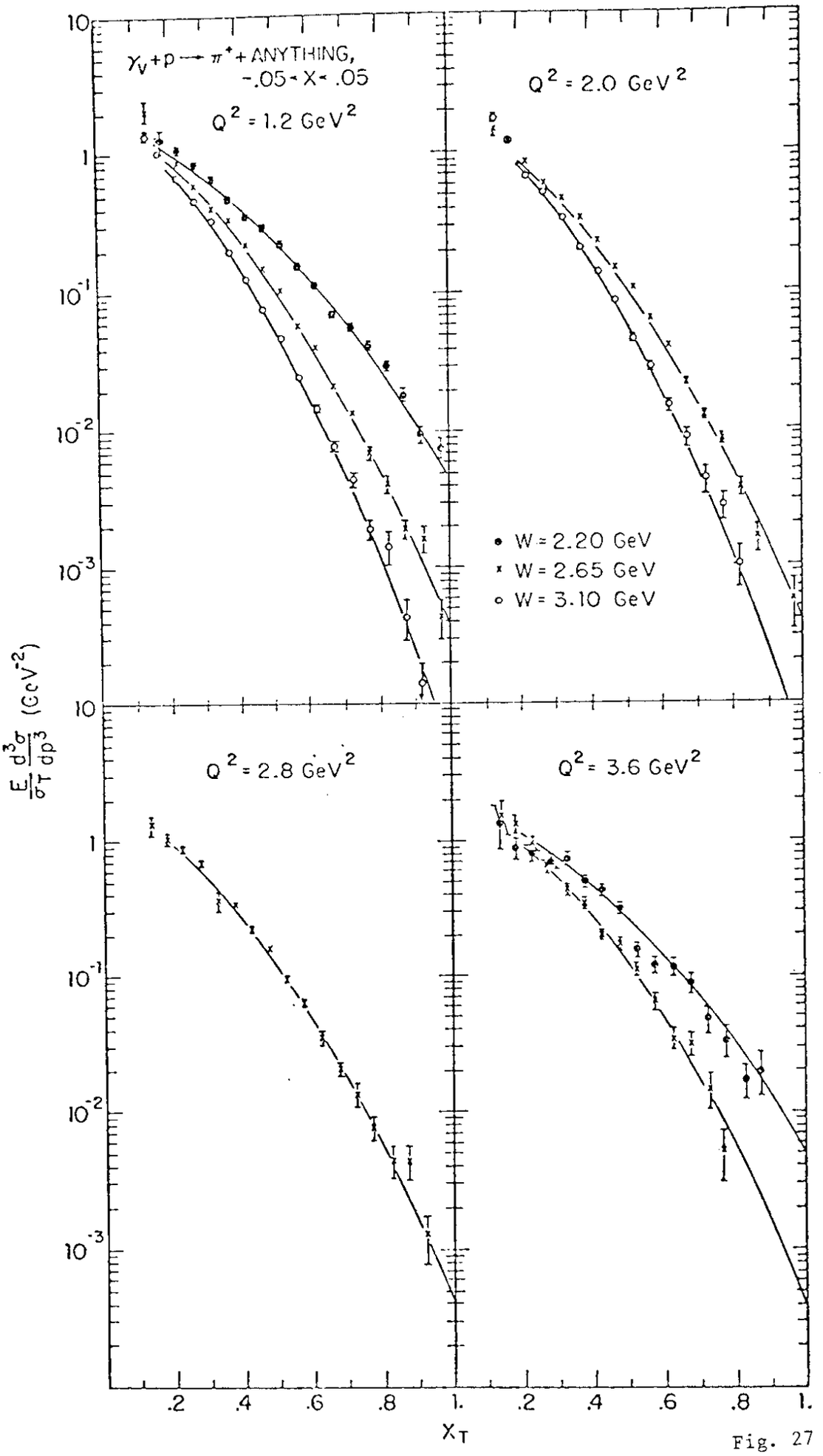
$\gamma_V + p \rightarrow \pi^+ + \text{ANYTHING}$,
$-.05 < X < .05$
$Q^2 = 1.2$ GeV$^2$
$Q^2 = 2.0$ GeV$^2$
$Q^2 = 2.8$ GeV$^2$
$Q^2 = 3.6$ GeV$^2$
W = 2.20 GeV
W = 2.65 GeV
W = 3.10 GeV
$\frac{E}{\sigma_T}\frac{d^3\sigma}{dp^3}$ (GeV$^{-2}$)
$X_T$

Fig. 27

23971

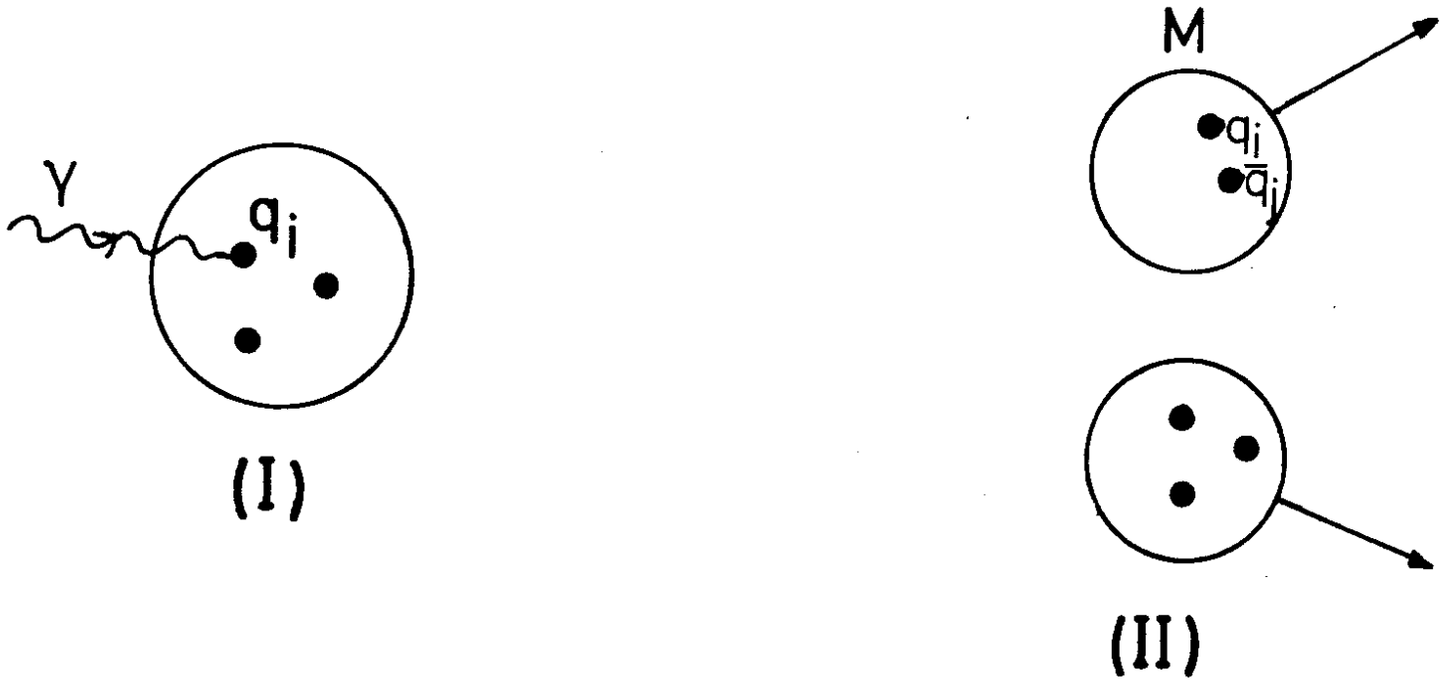


Fig. 28

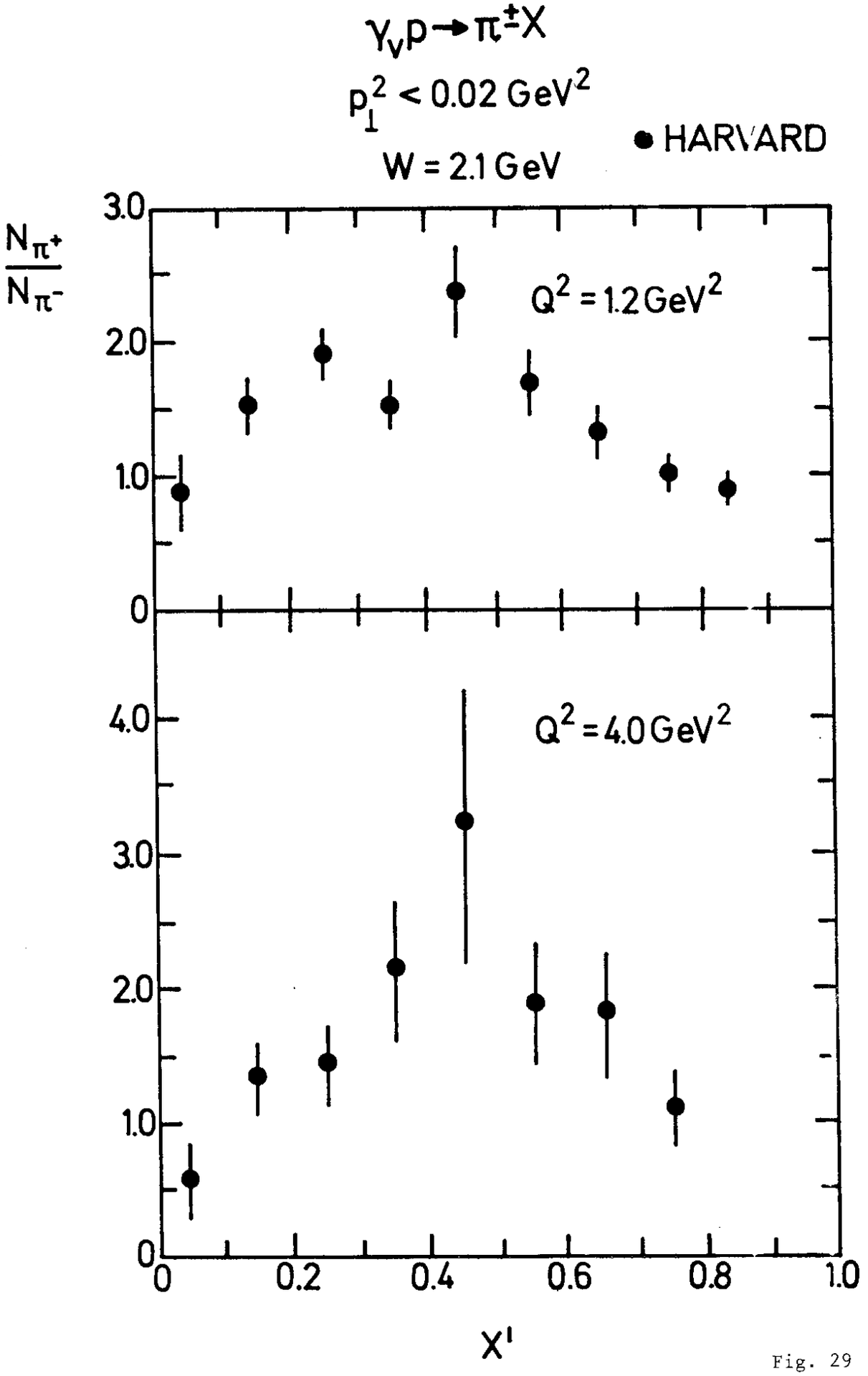
$\gamma_V p \to \pi^{\pm} X$
$p_\perp^2 < 0.02\ GeV^2$
W = 2.1 GeV
● HARVARD
$\frac{N_{\pi^+}}{N_{\pi^-}}$
$Q^2 = 1.2 GeV^2$
$Q^2 = 4.0 GeV^2$
3.0
2.0
1.0
0
4.0
3.0
2.0
1.0
0
0
0.2
0.4
0.6
0.8
1.0
X'

Fig. 29

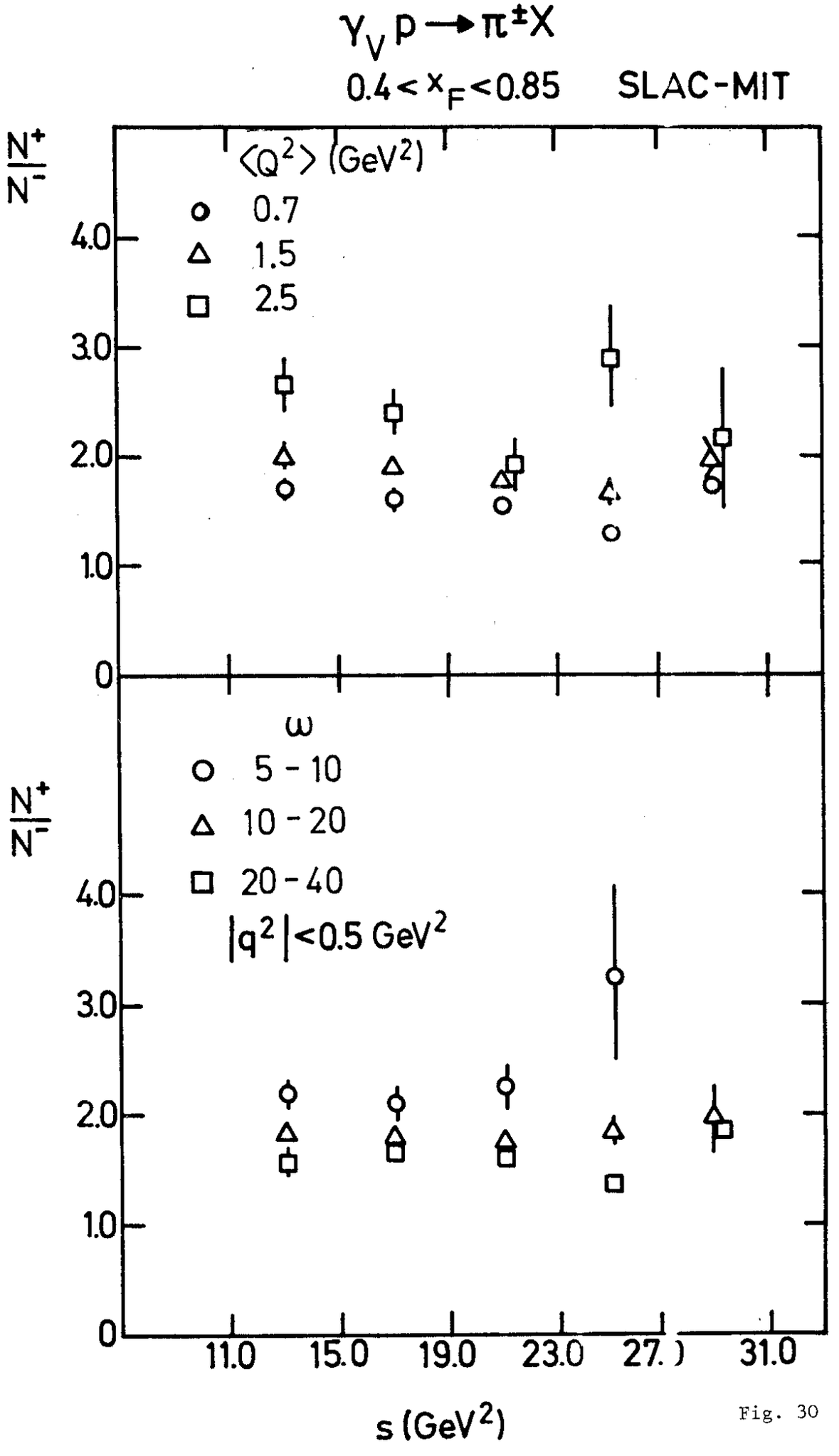
$\gamma_V p \rightarrow \pi^{\pm} X$
$0.4 < x_F < 0.85$ SLAC-MIT
$\frac{N^+}{N^-}$
$\langle Q^2 \rangle$ (GeV$^2$)
0.7
1.5
2.5
4.0
3.0
2.0
1.0
0
$\omega$
5 - 10
10 - 20
20 - 40
$|q^2| < 0.5$ GeV$^2$
11.0
15.0
19.0
23.0
27.0
31.0
s (GeV$^2$)

Fig. 30

$$\gamma_V p \longrightarrow h^{\pm} X$$

× $\pi^+/\pi^-$ DESY $s = 7\ GeV^2$ $0.4 < x < 0.7$

▲ $\pi^+/\pi^-$ Harvard $4 < s < 16\ GeV^2$ $0.3 < x < 0.7$

● $h^+/h^-$ SLAC-MIT $11 < s < 31\ GeV^2$ $0.4 < x < 0.85$

○ $h^+/h^-$ UCSC-SLAC $\nu > 2\ GeV$ $0.3 < x$

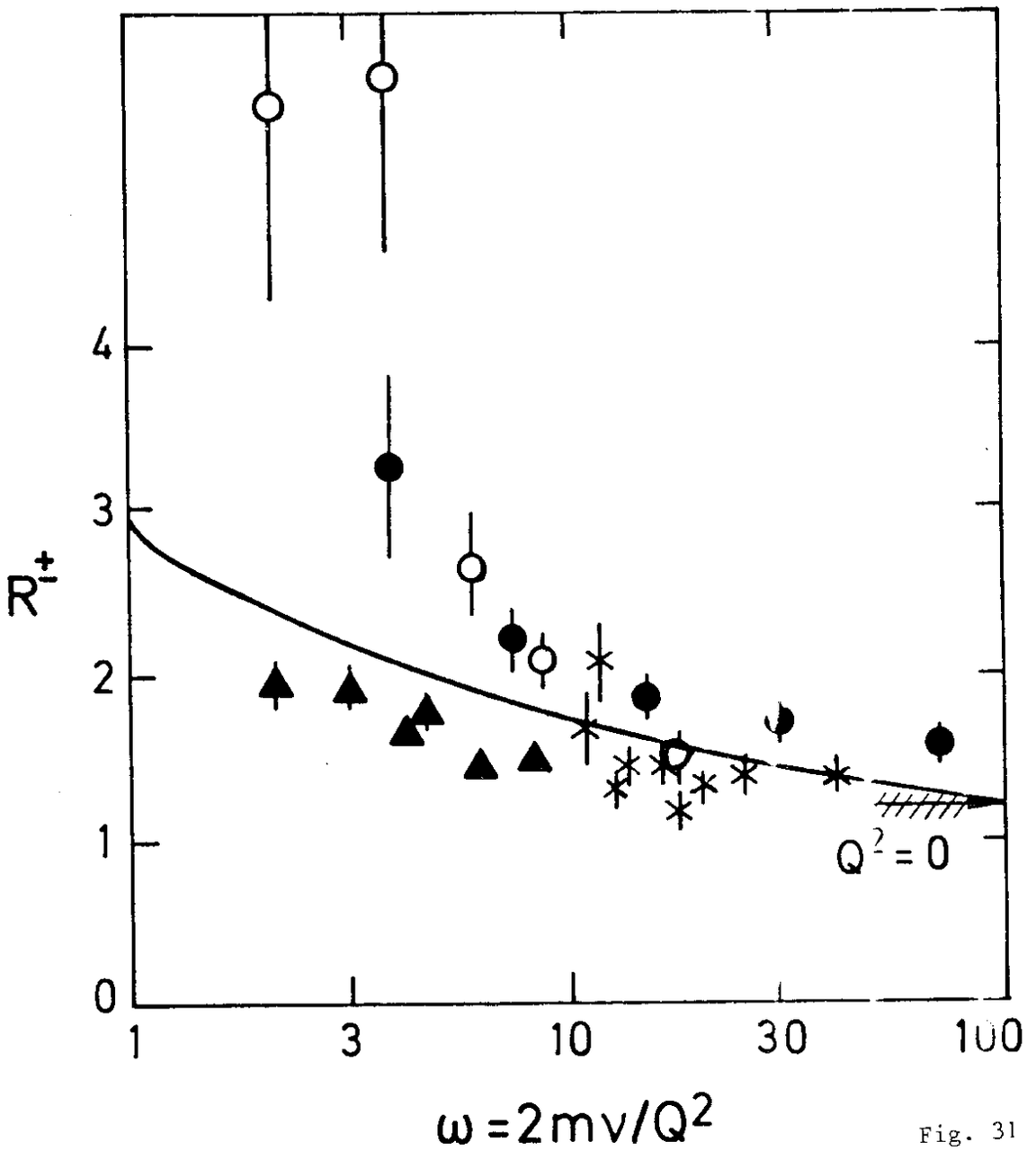


Fig. 31

$$\gamma_V n \longrightarrow h^{\pm} X$$

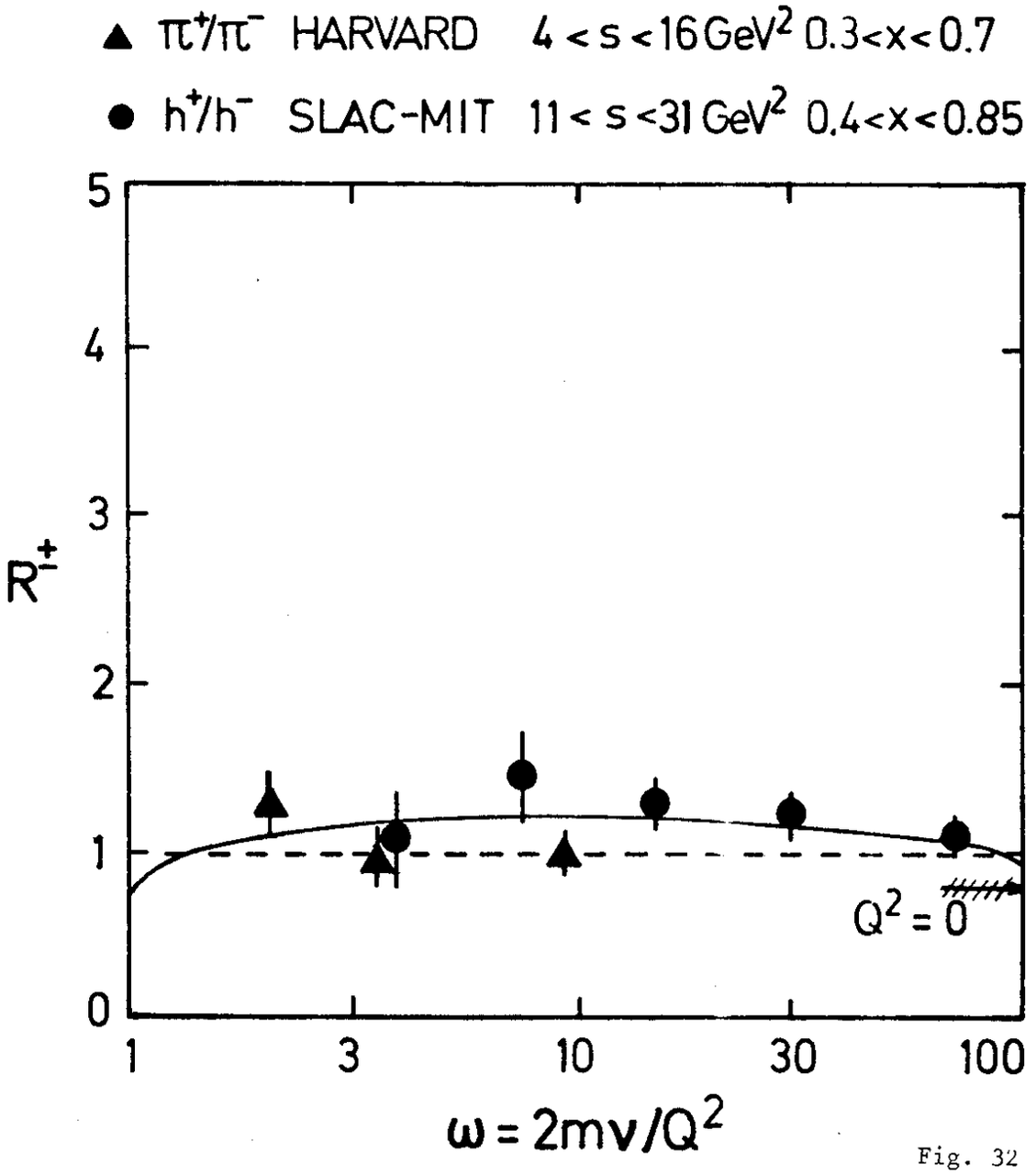


Fig. 32

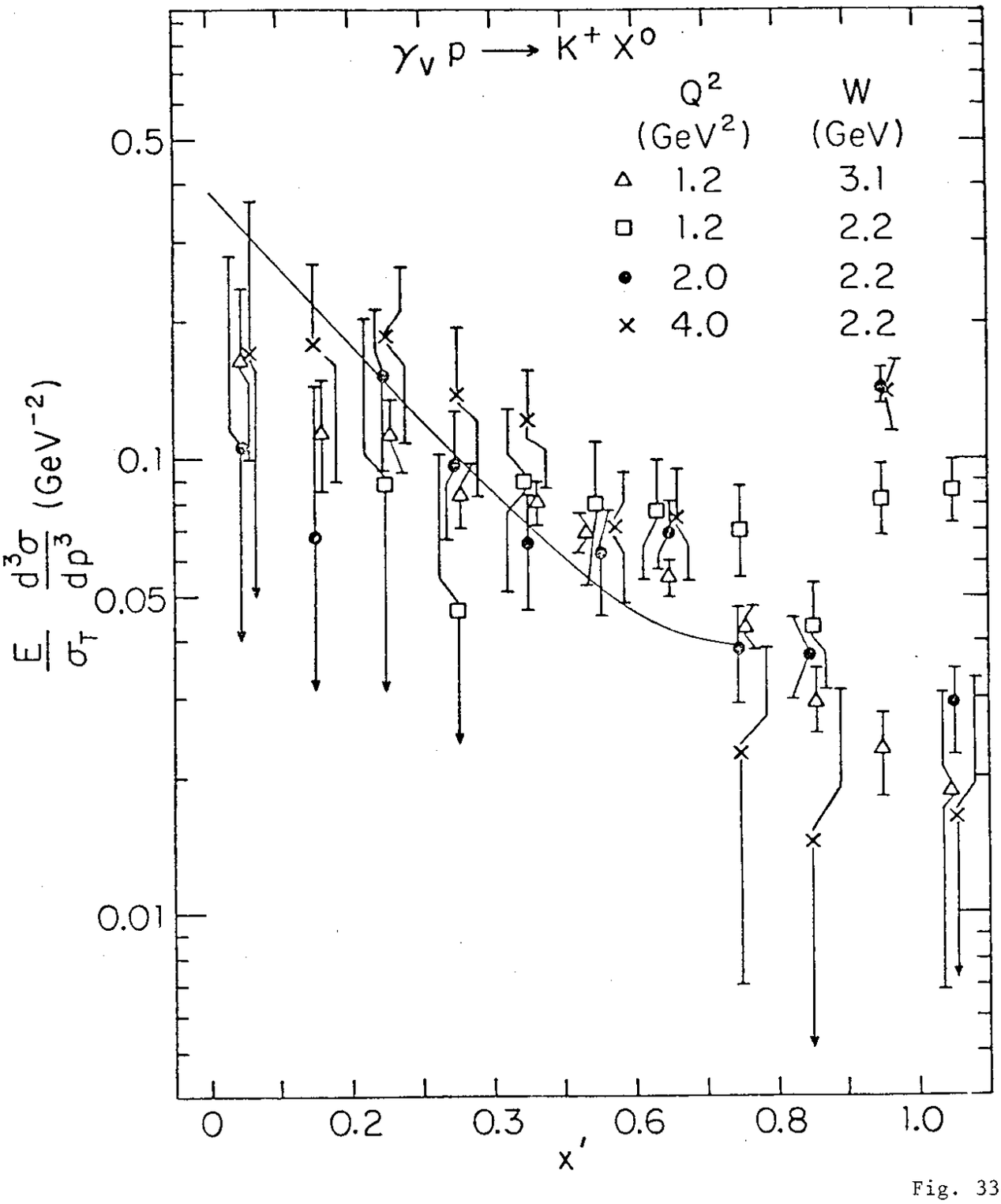
$\gamma_V p \longrightarrow K^+ X^o$
$Q^2$ (GeV$^2$)
W (GeV)
1.2 3.1
1.2 2.2
2.0 2.2
4.0 2.2
$\frac{E}{\sigma_T}\frac{d^3\sigma}{dp^3}$ (GeV$^{-2}$)
0.5
0.1
0.05
0.01
0
0.2
0.3
0.6
0.8
1.0
x'

Fig. 33

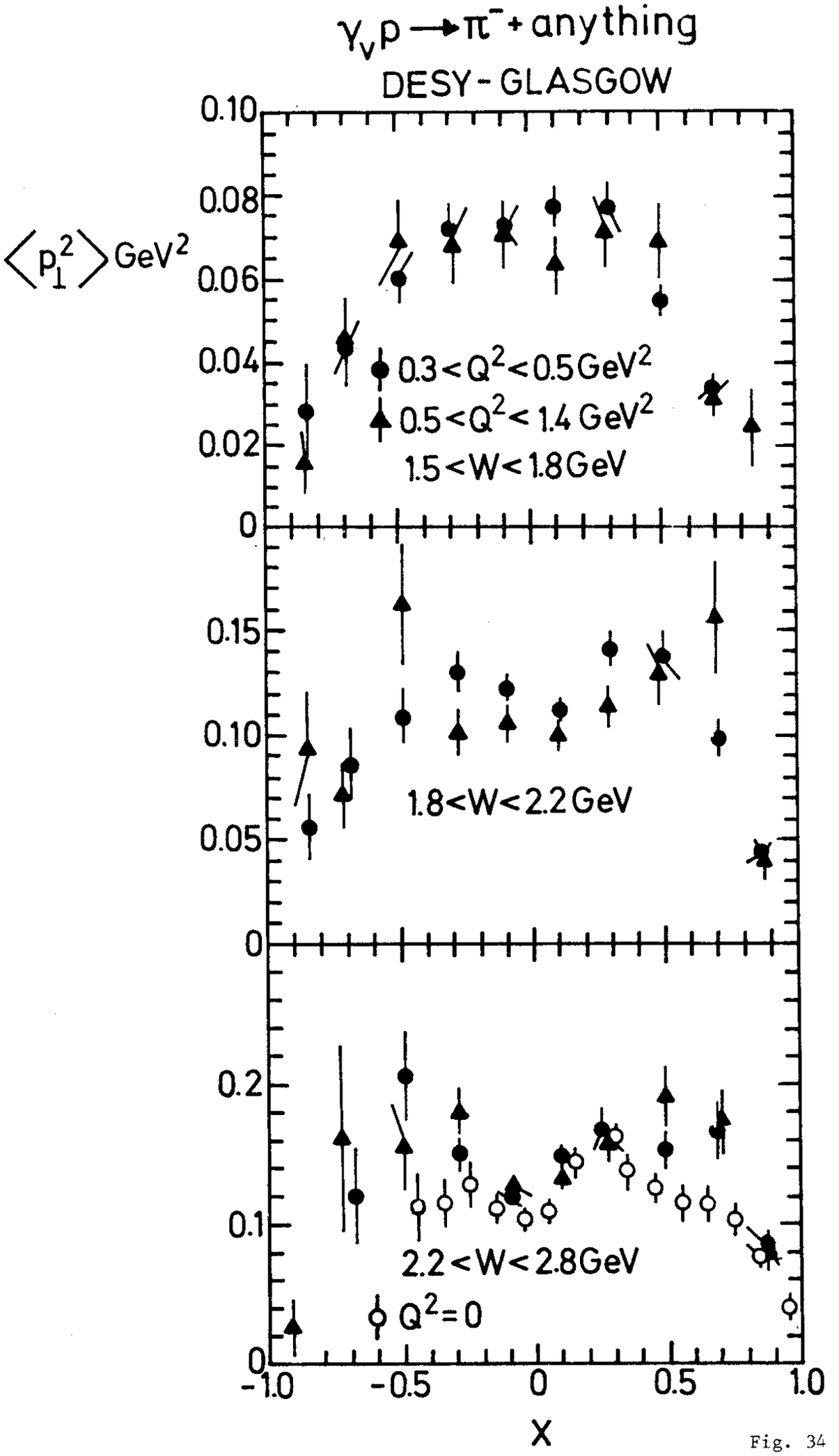
$\gamma_v p \rightarrow \pi^- +$ anything
DESY - GLASGOW
$\langle p_\perp^2 \rangle$ GeV$^2$
0.10
0.08
0.06
0.04
0.02
0
$0.3 < Q^2 < 0.5$ GeV$^2$
$0.5 < Q^2 < 1.4$ GeV$^2$
$1.5 < W < 1.8$ GeV
0.15
0.10
0.05
0
$1.8 < W < 2.2$ GeV
0.2
0.1
0
$2.2 < W < 2.8$ GeV
$Q^2 = 0$
-1.0
-0.5
0
0.5
1.0
X

Fig. 34

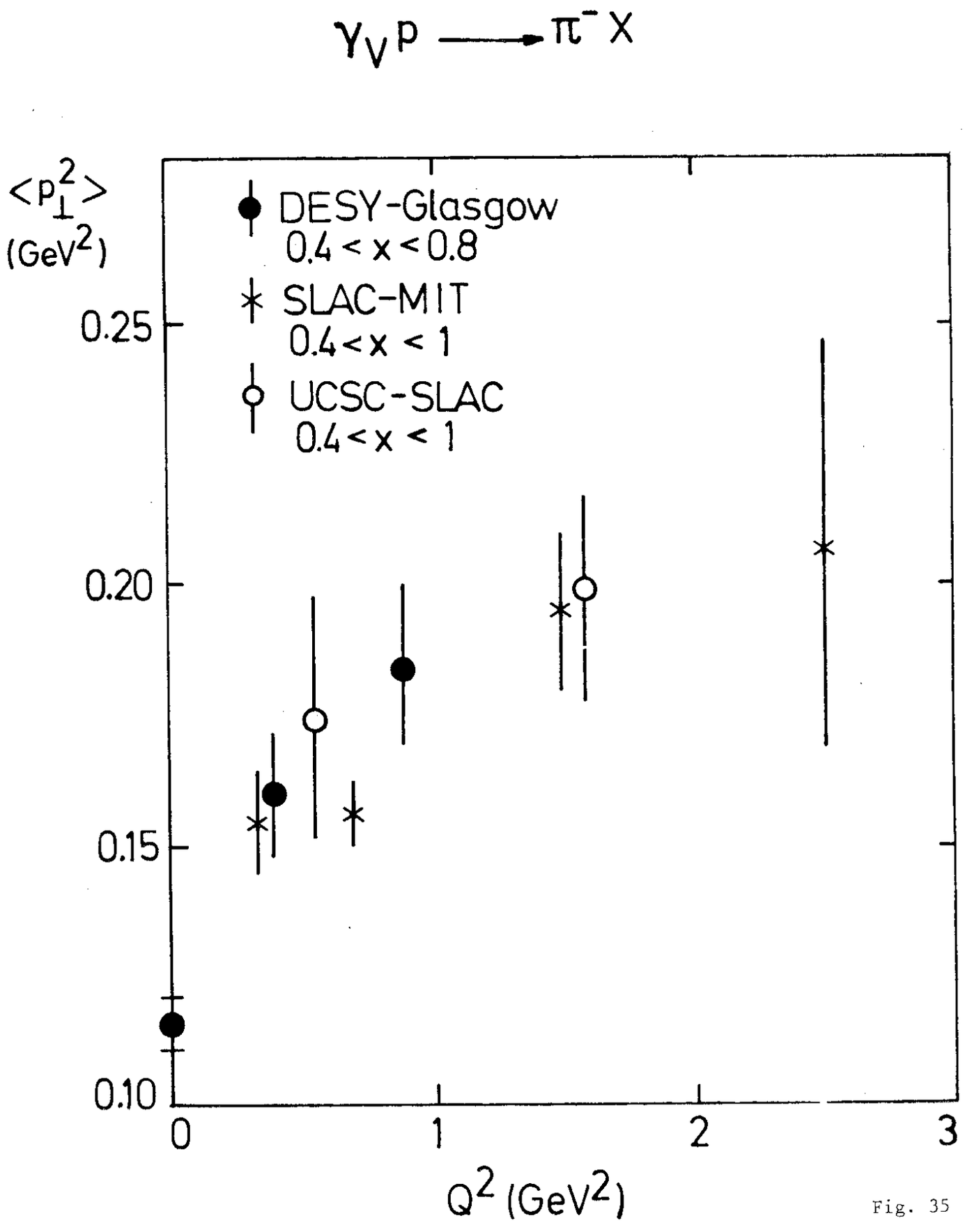
$\gamma_V p \longrightarrow \pi^- X$
$\langle p_\perp^2 \rangle$ (GeV$^2$)
DESY-Glasgow
0.4 < x < 0.8
SLAC-MIT
0.4 < x < 1
UCSC-SLAC
0.4 < x < 1
0.25
0.20
0.15
0.10
0
1
2
3
$Q^2$ (GeV$^2$)

Fig. 35

SLOPE PARAMETER IN HADRON ELECTROPRODUCTION

$e^{-Ap_T^2}$

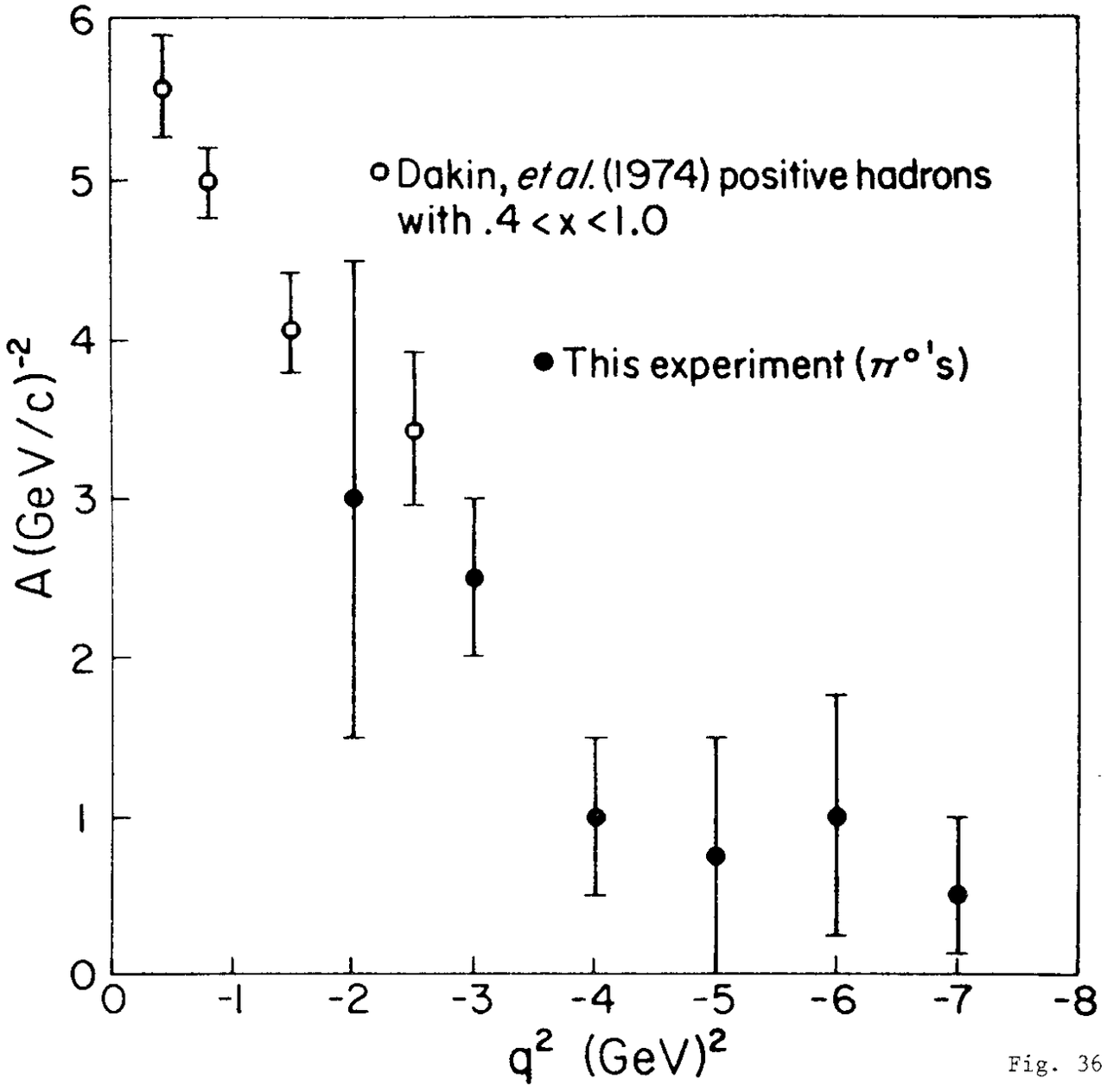


Fig. 36

23972

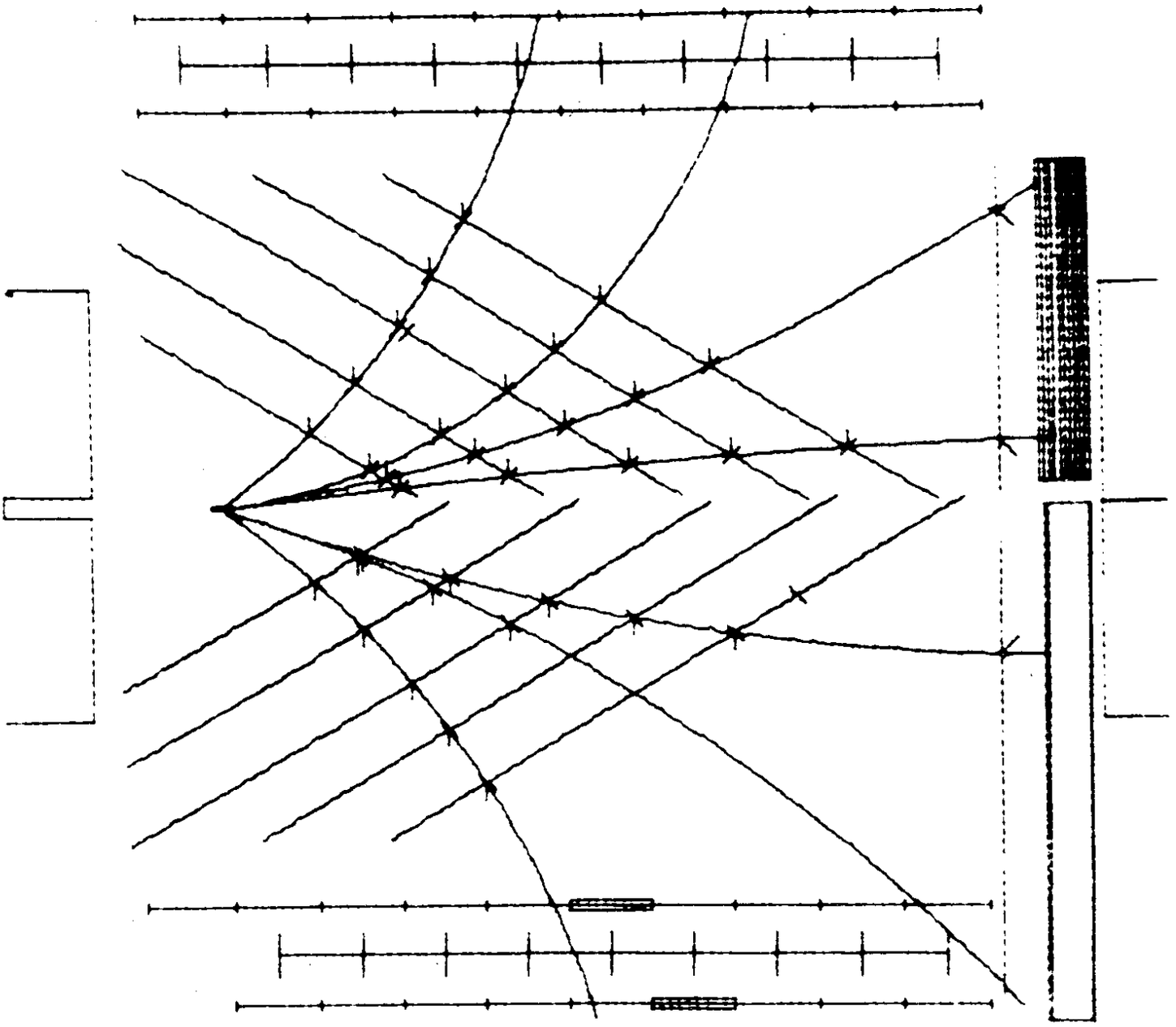


Fig. 37

23974